Fermilab FERMILAB-Pub-01/211-E CDF August 2001

Charged Jet Evolution and the Underlying Event in Proton-Antiproton Collisions at 1.8 TeV

T. Affolder,[23] H. Akimoto,[45] A. Akopian,[37] M. G. Albrow,[11] P. Amaral,[8] D. Amidei,[25] K. Anikeev,[24] J. Antos,[1] G. Apollinari,[11] T. Arisawa,[45] A. Artikov,[9] T. Asakawa,[43] W. Ashmanskas,[8] F. Azfar,[30] P. Azzi-Bacchetta,[31] N. Bacchetta,[31] H. Bachacou,[23] S. Bailey,[16] P. de Barbaro,[36] A. Barbaro-Galtieri,[23] V. E. Barnes,[35] B. A. Barnett,[19] S. Baroiant,[5] M. Barone,[13] G. Bauer,[24] F. Bedeschi,[33] S. Belforte,[42] W. H. Bell,[15] G. Bellettini,[33] J. Bellinger,[46] D. Benjamin,[10] J. Bensinger,[4] A. Beretvas,[11] J. P. Berge,[11] J. Berryhill,[8] A. Bhatti,[37] M. Binkley,[11] D. Bisello,[31] M. Bishai,[11] R. E. Blair,[2] C. Blocker,[4] K. Bloom,[25] B. Blumenfeld,[19] S. R. Blusk,[36] A. Bocci,[37] A. Bodek,[36] W. Bokhari,[32] G. Bolla,[35] Y. Bonushkin,[6] D. Bortoletto,[35] J. Boudreau,[34] A. Brandl,[27] S. van den Brink,[19] C. Bromberg,[26] M. Brozovic,[10] E. Brubaker,[23] N. Bruner,[27] E. Buckley-Geer,[11] J. Budagov,[9] H. S. Budd,[36] K. Burkett,[16] G. Busetto,[31] A. Byon-Wagner,[11] K. L. Byrum,[2] S. Cabrera,[10] P. Calafiura,[23] M. Campbell,[25] W. Carithers,[23] J. Carlson,[25] D. Carlsmith,[46] W. Caskey,[5] A. Castro,[3] D. Cauz,[42] A. Cerri,[33] A. W. Chan,[1] P. S. Chang,[1] P. T. Chang,[1] J. Chapman,[25] C. Chen,[32] Y. C. Chen,[1] M. -T. Cheng,[1] M. Chertok,[5] G. Chiarelli,[33] I. Chirikov-Zorin,[9] G. Chlachidze,[9] F. Chlebana,[11] L. Christofek,[18] M. L. Chu,[1] Y. S. Chung,[36] C. I. Ciobanu,[28] A. G. Clark,[14] A. Connolly,[23] J. Conway,[38] M. Cordelli,[13] J. Cranshaw,[40] R. Cropp,[41] R. Culbertson,[11] D. Dagenhart,[44] S. D'Auria,[15] F. DeJongh,[11] S. Dell'Agnello,[13] M. Dell'Orso,[33] L. Demortier,[37] M. Deninno,[3] P. F. Derwent,[11] T. Devlin,[38] J. R. Dittmann,[11] A. Dominguez,[23] S. Donati,[33] J. Done,[39] M. D'Onofrio,[33] T. Dorigo,[16] N. Eddy,[18] K. Einsweiler,[23] J. E. Elias,[11] E. Engels, Jr.,[34] R. Erbacher,[11] D. Errede,[18] S. Errede,[18] Q. Fan,[36] R. G. Feild,[47] J. P. Fernandez,[11] C. Ferretti,[33] R. D. Field,[12] I. Fiori,[3] B. Flaugher,[11] G. W. Foster,[11] M. Franklin,[16] J. Freeman,[11] J. Friedman,[24] Y. Fukui,[22] I. Furic,[24] S. Galeotti,[33] A. Gallas,[(**) 16] M. Gallinaro,[37] T. Gao,[32] M. Garcia-Sciveres,[23] A. F. Garfinkel,[35] P. Gatti,[31] C. Gay,[47] D. W. Gerdes,[25] P. Giannetti,[33] V. Glagolev,[9] D. Glenzinski,[11] M. Gold,[27] J. Goldstein,[11] I. Gorelov,[27] A. T. Goshaw,[10] Y. Gotra,[34] K. Goulianos,[37] C. Green,[35] G. Grim,[5] P. Gris,[11] L. Groer,[38] C. Grosso-Pilcher,[8] M. Guenther,[35] G. Guillian,[25] J. Guimaraes da Costa,[16] R. M. Haas,[12] C. Haber,[23] S. R. Hahn,[11] C. Hall,[16] T. Handa,[17] R. Handler,[46] W. Hao,[40] F. Happacher,[13] K. Hara,[43] A. D. Hardman,[35] R. M. Harris,[11] F. Hartmann,[20] K. Hatakeyama,[37] J. Hauser,[6] J. Heinrich,[32] A. Heiss,[20] M. Herndon,[19] C. Hill,[5] K. D. Hoffman,[35] C. Holck,[32] R. Hollebeek,[32] L. Holloway,[18] R. Hughes,[28] J. Huston,[26] J. Huth,[16] H. Ikeda,[43] J. Incandela,[11] G. Introzzi,[33] J. Iwai,[45] Y. Iwata,[17] E. James,[25] M. Jones,[32] U. Joshi,[11] H. Kambara,[14] T. Kamon,[39] T. Kaneko,[43] K. Karr,[44] H. Kasha,[47] Y. Kato,[29] T. A. Keaffaber,[35] K. Kelley,[24] M. Kelly,[25] R. D. Kennedy,[11] R. Kephart,[11] D. Khazins,[10] T. Kikuchi,[43] B. Kilminster,[36] B. J. Kim,[21] D. H. Kim,[21] H. S. Kim,[18] M. J. Kim,[21] S. B. Kim,[21] S. H. Kim,[43] Y. K. Kim,[23] M. Kirby,[10] M. Kirk,[4] L. Kirsch,[4] S. Klimenko,[12] P. Koehn,[28] K. Kondo,[45] J. Konigsberg,[12] A. Korn,[24] A. Korytov,[12] E. Kovacs,[2] J. Kroll,[32] M. Kruse,[10] S. E. Kuhlmann,[2] K. Kurino,[17] T. Kuwabara,[43] A. T. Laasanen,[35] N. Lai,[8] S. Lami,[37] S. Lammel,[11] J. Lancaster,[10] M. Lancaster,[23] R. Lander,[5] A. Lath,[38] G. Latino,[33] T. LeCompte,[2] A. M. Lee IV,[10] K. Lee,[40] S. Leone,[33] J. D. Lewis,[11] M. Lindgren,[6] T. M. Liss,[18] J. B. Liu,[36] Y. C. Liu,[1] D. O. Litvintsev,[11] O. Lobban,[40] N. Lockyer,[32] J. Loken,[30] M. Loreti,[31] D. Lucchesi,[31] P. Lukens,[11] S. Lusin,[46] L. Lyons,[30] J. Lys,[23] R. Madrak,[16] K. Maeshima,[11] P. Maksimovic,[16] L. Malferrari,[3] M. Mangano,[33] M. Mariotti,[31] G. Martignon,[31] A. Martin,[47] J. A. J. Matthews,[27] J. Mayer,[41] P. Mazzanti,[3] K. S. McFarland,[36] P. McIntyre,[39] E. McKigney,[32] M. Menguzzato,[31] A. Menzione,[33] C. Mesropian,[37] A. Meyer,[11] T. Miao,[11] R. Miller,[26] J. S. Miller,[25] H. Minato,[43] S. Miscetti,[13] M. Mishina,[22] G. Mitselmakher,[12] N. Moggi,[3] E. Moore,[27] R. Moore,[25] Y. Morita,[22] T. Moulik,[35] M. Mulhearn,[24] A. Mukherjee,[11] T. Muller,[20] A. Munar,[33] P. Murat,[11] S. Murgia,[26] J. Nachtman,[6] V. Nagaslaev,[40] S. Nahn,[47] H. Nakada,[43] I. Nakano,[17] C. Nelson,[11] T. Nelson,[11] C. Neu,[28] D. Neuberger,[20] C. Newman-Holmes,[11] C.-Y. P. Ngan,[24] H. Niu,[4] L. Nodulman,[2] A. Nomerotski,[12] S. H. Oh,[10] Y. D. Oh,[21] T. Ohmoto,[17] T. Ohsugi,[17] R. Oishi,[43] T. Okusawa,[29] J. Olsen,[46] W. Orejudos,[23] C. Pagliarone,[33] F. Palmonari,[33] R. Paoletti,[33] V. Papadimitriou,[40] D. Partos,[4] J. Patrick,[11] G. Pauletta,[42] M. Paulini,[(*) 23] C. Paus,[24] D. Pellett,[5] L. Pescara,[31] T. J. Phillips,[10] G. Piacentino,[33] K. T. Pitts,[18] A. Pompos,[35] L. Pondrom,[46] G. Pope,[34] M. Popovic,[41] F. Prokoshin,[9] J. Proudfoot,[2] F. Ptohos,[13] O. Pukhov,[9] G. Punzi,[33] A. Rakitine,[24] F. Ratnikov,[38] D. Reher,[23] A. Reichold,[30] A. Ribon,[31] W. Riegler,[16] F. Rimondi,[3] L. Ristori,[33] M. Riveline,[41] W. J. Robertson,[10] A. Robinson,[41] T. Rodrigo,[7] S. Rolli,[44] L. Rosenson,[24] R. Roser,[11] R. Rossin,[31] C. Rott,[35] A. Roy,[35] A. Ruiz,[7] A. Safonov,[5] R. St. Denis,[15] W. K. Sakumoto,[36] D. Saltzberg,[6] C. Sanchez,[28] A. Sansoni,[13] L. Santi,[42] H. Sato,[43] P. Savard,[41] P. Schlabach,[11] E. E. Schmidt,[11] M. P. Schmidt,[47] M. Schmitt,[(**) 16] L. Scodellaro,[31] A. Scott,[6] A. Scribano,[33] S. Segler,[11] S. Seidel,[27] Y. Seiya,[43] A. Semenov,[9] F. Semeria,[3] T. Shah,[24] M. D. Shapiro,[23] P. F. Shepard,[34] T. Shibayama,[43] M. Shimojima,[43] M. Shochet,[8] A. Sidoti,[31] J. Siegrist,[23] A. Sill,[40] P. Sinervo,[41] P. Singh,[18] A. J. Slaughter,[47] K. Sliwa,[44] C. Smith,[19] F. D. Snider,[11] A. Solodsky,[37] J. Spalding,[11] T. Speer,[14] P. Sphicas,[24] F. Spinella,[33] M. Spiropulu,[16] L. Spiegel,[11] J. Steele,[46] A. Stefanini,[33] J. Strologas,[18] F. Strumia, [14] D. Stuart,[11] K. Sumorok,[24] T. Suzuki,[43] T. Takano,[29] R. Takashima,[17] K. Takikawa,[43] P. Tamburello,[10] M. Tanaka,[43] B. Tannenbaum,[6] M. Tecchio,[25] R. Tesarek,[11] P. K. Teng,[1] K. Terashi,[37] S. Tether,[24] A. S. Thompson,[15] R. Thurman-Keup,[2] P. Tipton,[36] S. Tkaczyk,[11] D. Toback,[39] K. Tollefson,[36] A. Tollestrup,[11]

D. Tonelli,[33] H. Toyoda,[29] W. Trischuk,[41] J. F. de Troconiz,[16] J. Tseng,[24] N. Turini,[33] F. Ukegawa,[43] T. Vaiciulis,[36] J. Valls,[38] S. Vejcik III,[11] G. Velev,[11] G. Veramendi,[23] R. Vidal,[11] I. Vila,[7] R. Vilar,[7] I. Volobouev,[23] M. von der Mey,[6] D. Vucinic,[24] R. G. Wagner,[2] R. L. Wagner,[11] N. B. Wallace,[38] Z. Wan,[38] C. Wang,[10] M. J. Wang,[1] B. Ward,[15] S. Waschke,[15] T. Watanabe,[43] D. Waters,[30] T. Watts,[38] R. Webb,[39] H. Wenzel,[20] W. C. Wester III,[11] A. B. Wicklund,[2] E. Wicklund,[11] T. Wilkes,[5] H. H. Williams,[32] P. Wilson,[11] B. L. Winer,[28] D. Winn,[25] S. Wolbers,[11] D. Wolinski,[25] J. Wolinski,[26] S. Wolinski,[25] S. Worm,[27] X. Wu,[14] J. Wyss,[33] W. Yao,[23] G. P. Yeh,[11] P. Yeh,[1] J. Yoh,[11] C. Yosef,[26] T. Yoshida,[29] I. Yu,[21] S. Yu,[32] Z. Yu,[47] A. Zanetti,[42] F. Zetti,[23] and S. Zucchelli[3]

(CDF Collaboration)

[1] *Institute of Physics, Academia Sinica, Taipei, Taiwan 11529, Republic of China*
[2] *Argonne National Laboratory, Argonne, Illinois 60439*
[3] *Istituto Nazionale di Fisica Nucleare, University of Bologna, I-40127 Bologna, Italy*
[4] *Brandeis University, Waltham, Massachusetts 02254*
[5] *University of California at Davis, Davis, California 95616*
[6] *University of California at Los Angeles, Los Angeles, California 90024*
[7] *Instituto de Fisica de Cantabria, CSIC-University of Cantabria, 39005 Santander, Spain*
[8] *Enrico Fermi Institute, University of Chicago, Chicago, Illinois 60637*
[9] *Joint Institute for Nuclear Research, RU-141980 Dubna, Russia*
[10] *Duke University, Durham, North Carolina 27708*
[11] *Fermi National Accelerator Laboratory, Batavia, Illinois 60510*
[12] *University of Florida, Gainesville, Florida 32611*
[13] *Laboratori Nazionali di Frascati, Istituto Nazionale di Fisica Nucleare, I-00044 Frascati, Italy*
[14] *University of Geneva, CH-1211 Geneva 4, Switzerland*
[15] *Glasgow University, Glasgow G12 8QQ, United Kingdom*
[16] *Harvard University, Cambridge, Massachusetts 02138*
[17] *Hiroshima University, Higashi-Hiroshima 724, Japan*
[18] *University of Illinois, Urbana, Illinois 61801*
[19] *The Johns Hopkins University, Baltimore, Maryland 21218*
[20] *Institut für Experimentelle Kernphysik, Universität Karlsruhe, 76128 Karlsruhe, Germany*
[21] *Center for High Energy Physics: Kyungpook National University, Taegu 702-701; Seoul National University, Seoul 151-742; and SungKyunKwan University, Suwon 440-746; Korea*
[22] *High Energy Accelerator Research Organization (KEK), Tsukuba, Ibaraki 305, Japan*
[23] *Ernest Orlando Lawrence Berkeley National Laboratory, Berkeley, California 94720*
[24] *Massachusetts Institute of Technology, Cambridge, Massachusetts 02139*
[25] *University of Michigan, Ann Arbor, Michigan 48109*
[26] *Michigan State University, East Lansing, Michigan 48824*
[27] *University of New Mexico, Albuquerque, New Mexico 87131*
[28] *The Ohio State University, Columbus, Ohio 43210*
[29] *Osaka City University, Osaka 588, Japan*
[30] *University of Oxford, Oxford OX1 3RH, United Kingdom*
[31] *Universita di Padova, Istituto Nazionale di Fisica Nucleare, Sezione di Padova, I-35131 Padova, Italy*
[32] *University of Pennsylvania, Philadelphia, Pennsylvania 19104*
[33] *Istituto Nazionale di Fisica Nucleare, University and Scuola Normale Superiore of Pisa, I-56100 Pisa, Italy*
[34] *University of Pittsburgh, Pittsburgh, Pennsylvania 15260*
[35] *Purdue University, West Lafayette, Indiana 47907*
[36] *University of Rochester, Rochester, New York 14627*
[37] *Rockefeller University, New York, New York 10021*
[38] *Rutgers University, Piscataway, New Jersey 08855*
[39] *Texas A&M University, College Station, Texas 77843*
[40] *Texas Tech University, Lubbock, Texas 79409*
[41] *Institute of Particle Physics, University of Toronto, Toronto M5S 1A7, Canada*
[42] *Istituto Nazionale di Fisica Nucleare, University of Trieste/ Udine, Italy*
[43] *University of Tsukuba, Tsukuba, Ibaraki 305, Japan*
[44] *Tufts University, Medford, Massachusetts 02155*
[45] *Waseda University, Tokyo 169, Japan*
[46] *University of Wisconsin, Madison, Wisconsin 53706*

[47] *Yale University, New Haven, Connecticut 06520*
[(*)] *Now at Carnegie Mellon University, Pittsburgh, Pennsylvania 15213*
[(**)] *Now at Northwestern University, Evanston, Illinois 60208*

June 1, 2001

The growth and development of charged particle jets produced in proton-antiproton collisions at 1.8 TeV are studied. We see evidence of charged particle clusters (i.e., charged particle jets) in the Min-Bias data, which are consistent with a smooth continuation (down to small p_T) of the high transverse momentum charged jets observed in the JET20 data. A variety of leading (highest transverse momentum) charged jet observables are compared with the QCD hard scattering Monte-Carlo models HERWIG, ISAJET, and PYTHIA. The models describe fairly well the multiplicity distribution of charged particles within the leading charged jet, the size of the leading charged jet, the radial distribution of charged particles and transverse momentum around the leading charged jet direction, and the momentum distribution of charged particles within the leading charged jet. Also, a number of global observables are examined, where to fit the observable the QCD Monte-Carlo models have to describe correctly the overall proton-antiproton event structure. In particular, we study the behavior of the underlying event in hard scattering processes. None of the QCD models we examined (with its default parameters) describes correctly all the properties of the underlying event.

I. INTRODUCTION

In a proton-antiproton collision a large transverse momentum outgoing parton manifests itself as a cluster of particles (both charged and neutral) traveling in roughly the same direction. These clusters are referred to as "jets". In this paper we examine only the charged particle component of jets. Using a very simple algorithm, we study clusters of charged particles which we call charged particle jets. We define the transverse momentum of a charged particle jet to be the scalar sum of the transverse momenta of the charged particles making up the jet. We examine the properties of the leading (highest transverse momentum) charged particle jet and compare the data with the QCD hard scattering Monte-Carlo models HERWIG [1], ISAJET [2], and PYTHIA [3]. Here the Monte-Carlo models do not have to describe correctly the overall proton-antiproton event, just the leading charged particle jet. We study the growth and development of the leading (highest scalar p_T sum) charged particle jet, P_{T1}, from $P_{T1} = 0.5\,\mathrm{GeV/c}$ to $50\,\mathrm{GeV/c}$.

In addition to studying the leading charged particle jet, we study a variety of global observables, where to fit the observable the QCD Monte-Carlo models have to describe correctly the overall proton-antiproton event structure. In particular, we examine closely the behavior of the underlying event. A hard scattering event, like that illustrated in Fig. 1, consists of large transverse momentum outgoing hadrons that originate from the large transverse momentum partons (i.e., outgoing hard scattering jets) and also hadrons that originate from the break-up of the proton and antiproton (i.e., the beam-beam remnants). The underlying event is interesting but not well understood. In addition to beam-beam remnants, it may contain hadrons resulting from initial-state radiation. Also, it is possible that multiple parton scattering contributes to the underlying event as illustrated in Fig. 2. PYTHIA, for example, uses multiple parton interactions as a way to enhance the activity of the underlying event [3].

We examine charged particle correlations in the azimuthal angle ϕ. We use the direction of the leading charged particle jet in each event to define a region of η-ϕ space that is very sensitive to the underlying event, where η is the pseudo-rapidity. This "transverse" region is approximately normal to the plane of the hard 2-to-2 parton scattering. We find that the underlying event in a hard scattering is not the same as a soft proton-antiproton collision. For the same available energy the underlying event in a hard scattering is considerably more active (i.e., higher charged particle density and more transverse momentum) than a soft collision. This is not surprising since a violent hard scattering has occurred. We find that HERWIG, ISAJET, and PYTHIA with their default parameters do not describe correctly all the properties of the underlying event. For example, none of the models produces the correct p_T dependence of the beam-beam remnant contribution to the underlying event. Making precise measurements in the collider environment requires a detailed understanding of the underlying event.

In Section II we discuss the data and the QCD Monte-Carlo models used in this analysis and we explain the procedure used to compare the models with the data. In Section III, we define charged particle jets as simple circular regions in η-ϕ space with radius $R = 0.7$ and study the growth and development of these jets. In Section IV, we examine a variety of global observables and in Section V we study the behavior of the underlying event. We reserve Section VI for summary and conclusions.

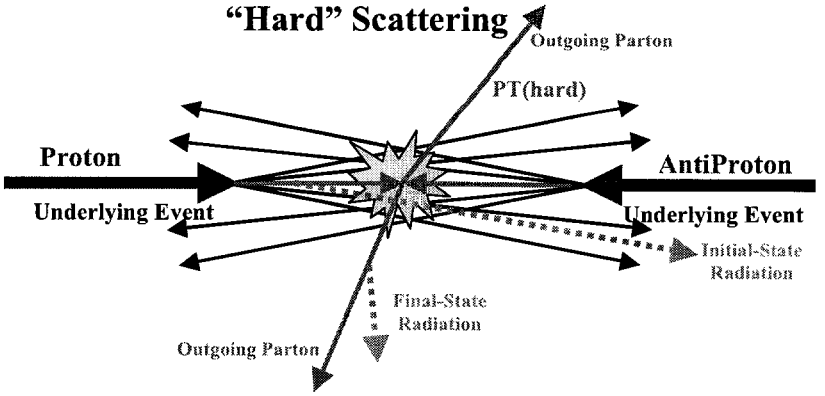

FIG. 1. Illustration of a proton-antiproton collision in which a hard 2-to-2 parton scattering with transverse momentum, p_T(hard), has occurred. The resulting event contains particles that originate from the two outgoing partons (plus final-state radiation) and particles that come from the breakup of the proton and antiproton (i.e., beam-beam remnants). The underlying event consists of the beam-beam remnants plus initial-state radiation.

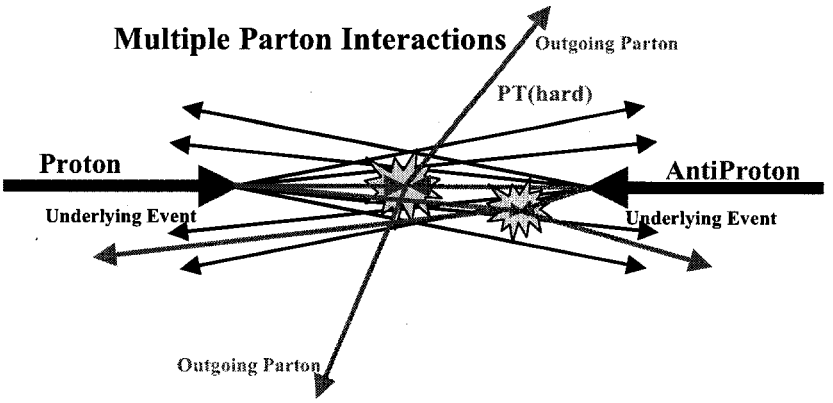

FIG. 2. Illustration of a proton-antiproton collision in which a multiple parton interaction has occurred. In addition to the hard 2-to-2 parton scattering with transverse momentum, p_T(hard), there is an additional soft or semi-hard parton-parton scattering that contributes particles to the underlying event. For PYTHIA, we include the particles that originate from soft or semi- hard multiple parton scatterings in the beam-beam remnant component.

TABLE I. Data sets and selection criterion used in this analysis.

CDF Data Set	Trigger	Events	Selection
Min-Bias	Min-Bias Trigger	626,966	zero or one vertex in $\lvert z\rvert < 100$ cm $\lvert z_c - z_v\rvert < 2$ cm, $\lvert d_0\rvert < 1$ cm $p_T > 0.5$ GeV/c, $\lvert\eta\rvert < 1$
JET20	Calorimeter Tower cluster with $E_T > 20$ GeV/c	78,682	zero or one vertex in $\lvert z\rvert < 100$ cm $\lvert z_c - z_v\rvert < 2$ cm, $\lvert d_0\rvert < 1$ cm $p_T > 0.5$ GeV/c, $\lvert\eta\rvert < 1$

II. DATA SELECTION AND MONTE-CARLO MODELS

A. Data Selection

The CDF detector, described in detail in Ref. [4], measures the trajectories and transverse momenta, p_T, of charged particles contained within the central tracking chamber (CTC), silicon vertex detector (SVX), and vertex time projection chamber (VTX), which are immersed in a 1.4 T solenoidal magnetic field. In this analysis we consider only charged particles measured by the CTC ($\delta p_T/p_T^2 \leq 0.002$ (GeV/c)$^{-1}$) and use the two trigger sets of data listed in Table 1. The minimum bias (min-bias) data were selected by requiring at least one particle interact with the forward beam-beam counter BBC ($3.4 < \eta < 5.9$) and at least one particle interact with the backward BBC ($-5.9 < \eta < -3.4$).

To remain in a region of high track finding efficiency, we consider only charged particles with $p_T > 0.5$ GeV/c and $|\eta| < 1$. In general, the observed tracks include some spurious tracks that result from secondary interactions between primary particles, including neutral particles, and the detector material. There are also particles originating from other proton-antiproton collisions in the same bunch crossing. To reduce the contribution from these sources, we consider only tracks which point to the primary interaction vertex within 2 cm along the beam direction, z, and within 1 cm transverse the beam direction, d_0. Detector simulation studies indicate that this d_0 impact parameter cut is very efficient and that the number of spurious tracks is about 3.5% when a 1 cm impact parameter cut is applied in conjunction with a $\Delta z = 2$ cm vertex cut. Without the impact parameter cut the number of spurious tracks is approximately 9%.

This dependence of the number of spurious tracks on the impact parameter cut provides a method of estimating systematic uncertainties due to unwanted (i.e., fake) tracks. Every data point on every plot in this analysis was determined three times by using a 2 cm vertex cut in conjunction with three different d_0 cuts: a 1 cm d_0 cut; a 0.5 cm d_0 cut; and no d_0 cut. The 1 cm cut determined the value of the data point and the difference between the 0.5 cm cut value and the no cut value of the data point was used to estimate the systematic error. This systematic error was then added in quadrature with the statistical error. We do not correct the data for the track finding efficiency. Instead the Monte-Carlo model predictions are corrected for the track finding efficiency. These corrections are small (less than 10%) and essentially independent of p_T and η in the selected region. We have verified that this method of incorporating the effect of fake and missed tracks is consistent with more detailed and time consuming detector simulations.

B. QCD Hard Scattering Monte-Carlo Models

In this analysis, the data are compared with the QCD hard scattering Monte-Carlo models HERWIG 5.9, ISAJET 7.32, PYTHIA 6.115, and PYTHIA 6.125. The QCD perturbative 2-to-2 parton-parton differential cross section diverges as the transverse momentum of the scattering, p_T(hard), goes to zero. One must set a minimum p_T(hard) large enough so that the resulting cross section is not larger that the total inelastic cross section, and also large enough to ensure that QCD perturbation theory is applicable. In this analysis we take p_T(hard) > 3 GeV/c.

Each of the QCD Monte-Carlo approaches model the beam-beam remnants in slightly different ways. However, all the models assume that a hard scattering event is basically the superposition of a hard parton-parton interaction on top of a soft collision. HERWIG assumes that the underlying event is a soft collision between the two beam "clusters". ISAJET uses a model similar to the one it uses for soft min-bias events (i.e., "cut Pomeron"), but with different parameters, to describe the underlying beam-beam remnants. PYTHIA assumes that each incoming beam hadron leaves behind beam remnants, which do not radiate initial state radiation, and simply pass through unaffected by the hard process. However, unlike HERWIG and ISAJET, PYTHIA also uses multiple parton interactions to enhance the activity of the underlying event as illustrated in Fig. 2.

CDF data [5] show evidence for multiple parton collisions in which both interactions are hard. However, multiple parton collisions contribute to the underlying event when one scattering is hard (i.e., the outgoing jets) and one scattering is soft or semi-hard. This second semi- hard collision cannot be computed reliably by perturbation theory and must be modeled. The amount of multiple parton scattering in which one scattering is hard and the other is semi-hard is essentially arbitrary. In this analysis we examine two versions of PYTHIA, PYTHIA 6.115 and PYTHIA 6.125 both with the default values for all the parameters. The default values of the parameters are different in version 6.115 and 6.125. In particular, the effective minimum transverse momentum for multiple parton interactions, PARP(81), changed from 1.4 GeV/c in version 6.115 to 1.9 GeV/c in version 6.125. Increasing this cut-off decreases the multiple parton interaction cross section which reduces the amount of multiple parton scattering. For completeness, we also consider PYTHIA with no multiple parton scattering (MSTP(81)=0).

Since ISAJET employs independent fragmentation it is possible to trace particles back to their origin and divide them into three categories: particles that arise from the break-up of the beam particles (beam-beam remnants), particles that arise from initial-state radiation, and particles that result from the outgoing hard scattering jets plus final-state radiation. The hard scattering component consists of the particles that arise from the outgoing hard scattering jets plus initial and final-state radiation (the sum of the last two categories). Particles from the first two categories (beam-beam remnants plus initial-state radiation) are normally what is referred to as the underlying event. Of course, these categories are not directly distinguishable experimentally. Nevertheless, it is instructive to examine how particles from various origins affect the experimental observables.

Since PYTHIA does not use independent fragmentation, it is not possible to distinguish particles that arise from initial-state radiation from those that arise from final-state radiation, but we can identify the beam-beam remnants. When, for example, a color string breaks into hadrons it is not possible to say which of the two partons producing the string was the parent. For HERWIG and PYTHIA we divide particles into two categories: particles that arise from the break-up of the beam particles (beam-beam remnants), and particles that result from the outgoing hard scattering jets plus initial and final-state radiation (hard scattering component). For PYTHIA we include particles that arise from the soft or semi-hard scattering in multiple parton interactions in the beam-beam remnant component.

C. Method of Comparing the Monte-Carlo Models with Data

Our philosophy in comparing the QCD Monte-Carlo models with data is to select a region where the data are very clean. The track finding efficiency can vary substantially for very low p_T tracks and in dense high p_T jets. To avoid this we have considered only the region $p_T > 0.5\,\mathrm{GeV/c}$ and $|\eta| < 1$ where the track finding efficiency is high (estimated to be 92%) and stable and we restrict ourselves to charged particle jets with p_T less than $50\,\mathrm{GeV/c}$. The data presented here are uncorrected. Instead the Monte-Carlo models are corrected for the track finding efficiency and have an uncertainty (statistical plus systematic) of about 5%. The error bars on the (uncorrected) data include both statistical and correlated systematic uncertainties.

Restricting ourselves to the clean region $p_T > 0.5\,\mathrm{GeV/c}$ and $|\eta| < 1$ means, of course, that we see, on the average, only a small fraction of the total number of charged particles that are produced in the event. For example, of the 74 charged particles produced, on the average, by ISAJET (with $p_T(\mathrm{hard}) > 3\,\mathrm{GeV/c}$) at 1.8 TeV in proton-antiproton collisions about 25 have $p_T > 0.5\,\mathrm{GeV/c}$ and about 14 have $|\eta| < 1$ and only about 5 charged particles are, on the average, in the region $p_T > 0.5\,\mathrm{GeV/c}$ and $|\eta| < 1$. However, at large values of P_{T1} we are selecting events with many charged particles in the region $p_T > 0.5\,\mathrm{GeV/c}$ and $|\eta| < 1$ allowing us to study the topology of the event in detail.

In comparing the QCD hard scattering Monte-Carlo models with the data, we require that the Monte-Carlo events would satisfy the CDF min-bias trigger and we apply an 92% correction for the track finding efficiency (i.e., 8% of the charged tracks are, on the average, removed). Requiring the Monte-Carlo events to satisfy the min-bias trigger is important when comparing with the Min-Bias data, but does not matter when comparing with the JET20 data since essentially all high p_T jet events satisfy the min-bias trigger.

III. THE EVOLUTION OF CHARGED PARTICLE JETS

In this section, we define charged particle jets and examine the evolution of these jets from $P_{T1} = 0.5\,\mathrm{GeV/c}$ to $50\,\mathrm{GeV/c}$. As illustrated in Fig. 3, we define jets as clusters of charged particles in circular regions ($R = 0.7$) of η-ϕ space. They contain charged particles from the underlying event as well as particles which originate from the fragmentation of high p_T outgoing partons. Also every charged particle in the event is assigned to a jet, with the possibility that some jets might consist of just one charged particle. We use a simple, but non-standard jet definition since we will be dealing with jets that consist of only a few low p_T charged particles or even a single low p_T particle. The standard CDF jet algorithm based on calorimeter tower clustering is not directly applicable to charged particles. Furthermore, we need an algorithm that can be applied at low transverse momentum.

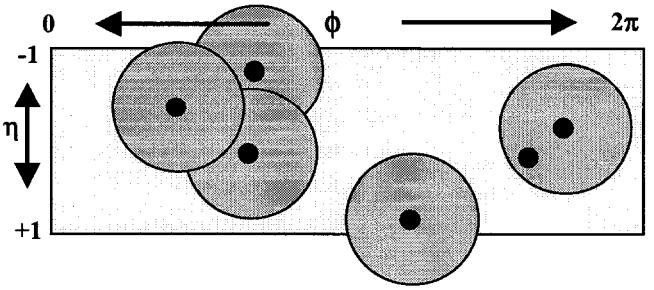

FIG. 3. Illustration of an event with six charged particles ($p_T > 0.5\,\mathrm{GeV/c}$ and $|\eta| < 1$) and five charged jets (circular regions in η-ϕ space with $R = 0.7$).

A. Charged Particle Jet Definition

We define jets as circular regions in η-ϕ space with radius defined by $R = \sqrt{(\Delta\eta)^2 + (\Delta\phi)^2}$. Our jet algorithm is as follows:

- Order all charged particles according to their p_T.
- Start with the highest p_T particle and include in the jet all particles within the radius $R = 0.7$ (considering each particle in the order of decreasing p_T and recalculating the centroid of the jet after each new particle is added to the jet).
- Go to the next highest p_T particle (not already included in a jet) and add to the jet all particles (not already included in a jet) within $R = 0.7$.
- Continue until all particles are in a jet.

We consider all charged particles ($p_T > 0.5\,\mathrm{GeV/c}$ and $|\eta| < 1$) and allow the jet radius to extend outside $|\eta| < 1$. Fig. 3 illustrates an event with six charged particles and five jets. We define the transverse momentum of the jet to be the scalar p_T sum of all the particles within the jet (i.e., it is simply the charged scalar p_T sum within the circular region). The maximum number of jets is related to the geometrical size of jets compared to the size of the region considered and is given approximately by

$$N_{jet}(\mathrm{max}) \approx 2\frac{(2)(2\pi)}{\pi(0.7)^2} \approx 16. \tag{1}$$

The additional factor of two is to allow for the overlap of jet radii as illustrated in Fig. 3.

We realize that the simple charged particle jet definition used here is not theoretically favored since if applied at the parton level it is not infrared safe. Of course, all jet definitions (and in fact all observables) are infrared safe at the hadron level. We have done a detailed study comparing the naive jet definition used here with a variety of more sophisticated charged particle jet definitions. Some of the observables presented here do, of course, depend on the definition of a jet and it is important to apply the same definition to both the QCD Monte-Carlo Models and the data.

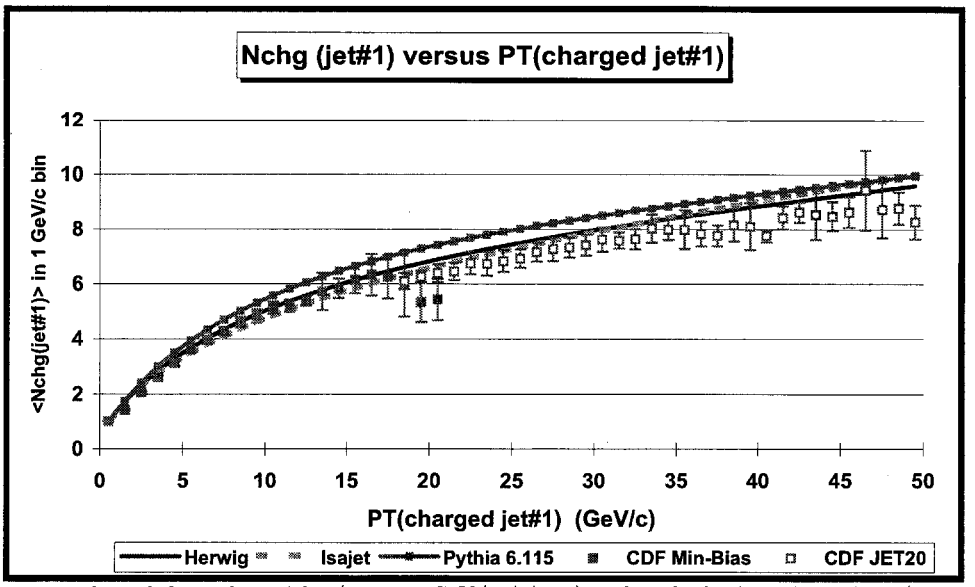

FIG. 4. The average number of charged particles ($p_T > 0.5\,\mathrm{GeV/c}$, $|\eta| < 1$) within the leading charged jet ($R = 0.7$) as a function of the p_T of the leading charged jet compared with the QCD hard scattering Monte-Carlo predictions of HERWIG, ISAJET, and PYTHIA 6.115. The solid (open) points are Min-Bias (JET20) data.

B. Charged Jet Multiplicity versus P_{T1}

Fig. 4 shows the average number of charged particles ($p_T > 0.5\,\mathrm{GeV/c}$ and $|\eta| < 1$) within chgjet#1 (leading charged jet) as a function of P_{T1}. The solid points are Min-Bias data and the open points are the JET20 data. The JET20 data connect smoothly to the Min-Bias data and allows us to study observables over the range $0.5\,\mathrm{GeV/c} < P_{T1} < 50\,\mathrm{GeV/c}$. There is a small overlap region where the Min-Bias and JET20 data agree. Of course, if we had a large enough sample of Min-Bias data, it would contain all the JET20 data. The errors on the data include both statistical and correlated systematic uncertainties, however the data have not been corrected for efficiency. Fig. 4 shows a sharp rise in the leading charged jet multiplicity at low P_{T1} and then more gradual rise at high P_{T1}. The data are compared with the QCD hard scattering Monte-Carlo predictions of HERWIG, ISAJET, and PYTHIA. The theory curves are corrected for the track finding efficiency and have an uncertainty (statistical plus systematic) of around 5%.

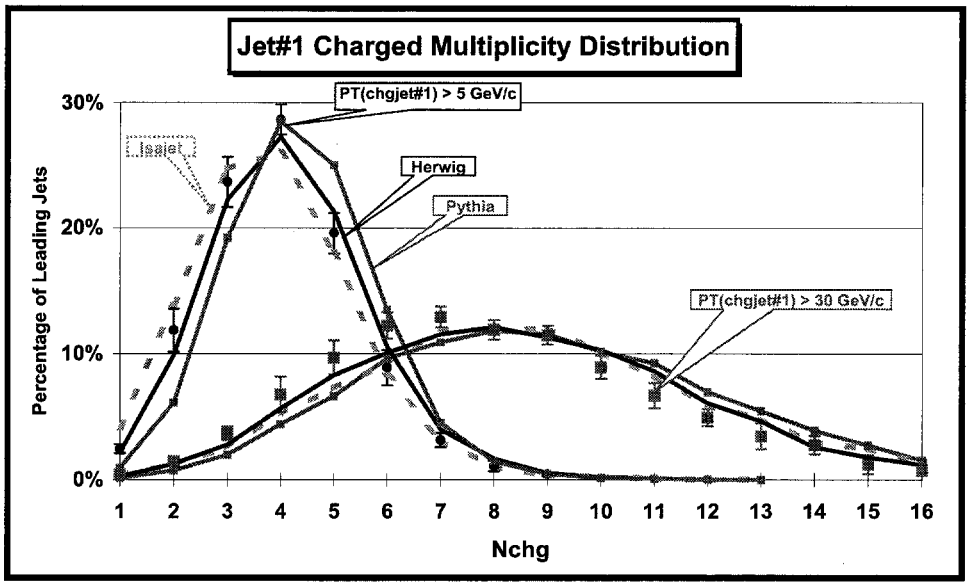

FIG. 5. Multiplicity distribution of charged particles ($p_T > 0.5\,\mathrm{GeV/c}$, $|\eta| < 1$) within chgjet#1 (leading charged jet) for $P_{T1} > 5$ and $30\,\mathrm{GeV/c}$ compared with the QCD hard scattering Monte-Carlo predictions of HERWIG, ISAJET, and PYTHIA 6.115. Plot shows the percentage of events in which the leading charged jet ($R = 0.7$) contains N_{chg} charged particles. The $P_{T1} > 5\,\mathrm{GeV/c}$ points are Min-Bias data and the $P_{T1} > 30\,\mathrm{GeV/c}$ points are JET20 data.

Fig. 5 shows the multiplicity distribution of the charged particles within chgjet#1 (leading charged jet) for $P_{T1} > 5\,\mathrm{GeV/c}$, and $30\,\mathrm{GeV/c}$ compared with the QCD hard scattering Monte- Carlo predictions. Below $5\,\mathrm{GeV/c}$ the probability that the leading charged jet consists of just one particle becomes large. The Monte-Carlo models agree fairly well with the data at both $5\,\mathrm{GeV/c}$ and $30\,\mathrm{GeV/c}$.

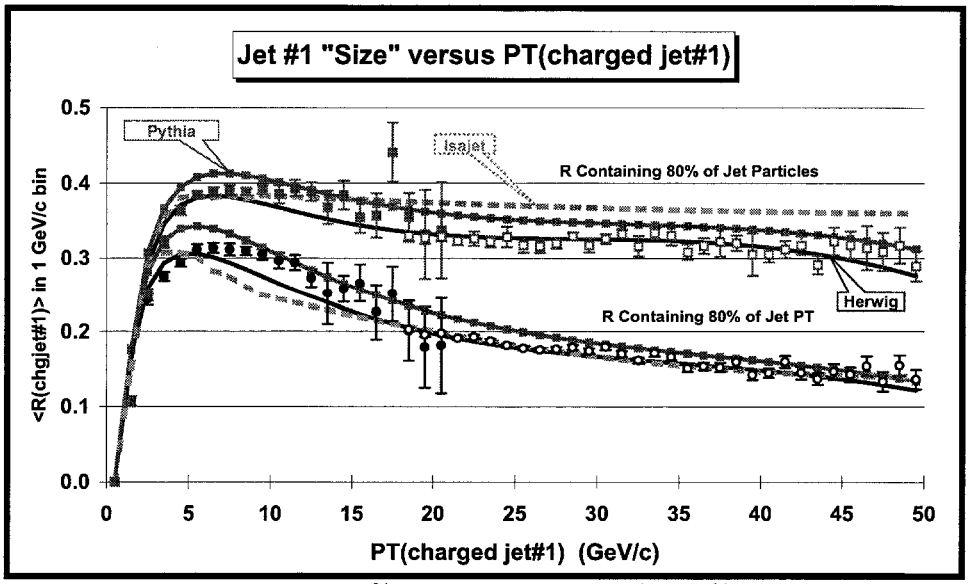

FIG. 6. The average radius in η-ϕ space containing 80% of the charged particles (and 80% of the charged scalar p_T sum) as a function of the transverse momentum of the leading charged jet compared with the QCD hard scattering Monte-Carlo predictions of HERWIG, ISAJET, and PYTHIA 6.115. The solid (open) points are Min-Bias (JET20) data.

C. Charged Jet Size versus P_{T1}

Although we defined jets as circular regions in η-ϕ space with $R = 0.7$, this is not the size of the jet. The size of a jet can be defined in two ways, according to particle number or according to transverse momentum. The first corresponds to the radius in η-ϕ space that contains 80% of the charged particles in the jet and the second corresponds to the radius in η-ϕ space that contains 80% of the jet transverse momentum. The data on the average jet size of the leading charged particle jet are compared with the QCD hard scattering Monte-Carlo predictions of HERWIG, ISAJET, and PYTHIA in Fig. 6. A leading $20\,\mathrm{GeV/c}$ charged jet has 80% of its charged particles contained, on the average, within a radius in η-ϕ space of about 0.33, and 80% of its transverse momentum contained, on the average, within a radius of about 0.20. Fig. 6 clearly illustrates the hot core of charged jets. The radius containing 80% of the transverse momentum is smaller than the radius that contains 80% of the particles. Furthermore, the radius containing 80% of the transverse momentum decreases as the overall transverse momentum of the jet increases due to limited momentum perpendicular to the jet direction.

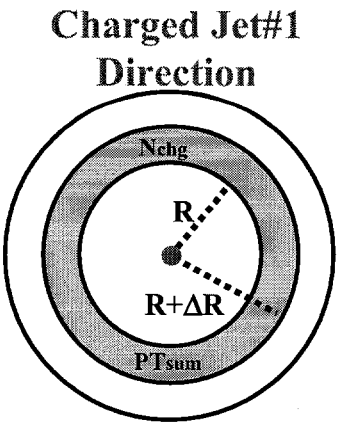

FIG. 7. Illustration of correlations in the radial distance R in η-ϕ space from the direction of the leading charged jet in the event, chgjet#1. The radius R is the distance in η-ϕ space between the leading charged jet and a charged particle, $R^2 = (\Delta\eta)^2 + (\Delta\phi)^2$. We plot $\langle N_{\rm chg}\rangle$ and $\langle P_T(\text{sum})\rangle$ in a $\Delta R = 0.02$ bin versus R.

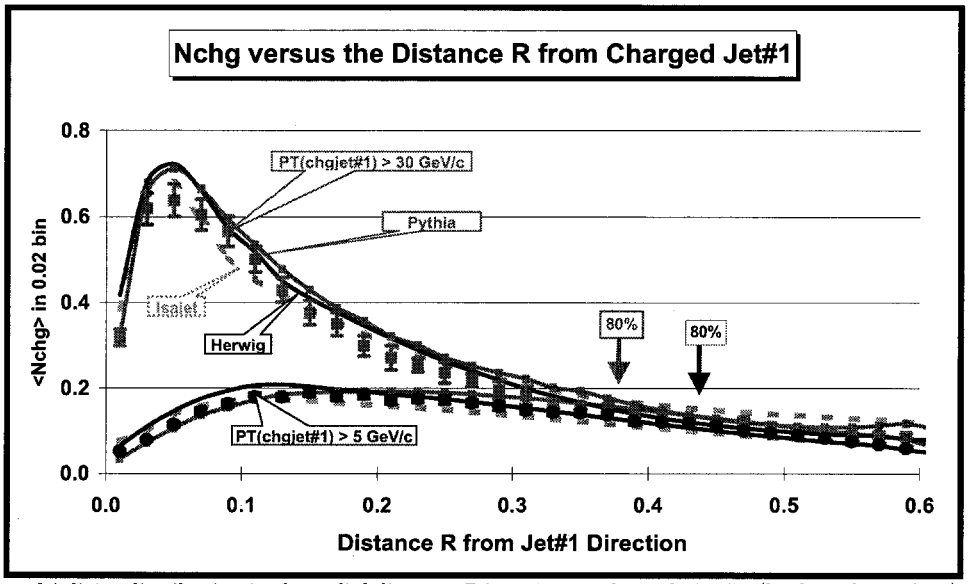

FIG. 8. Charged multiplicity distribution in the radial distance R in η-ϕ space from chgjet#1 (leading charged jet) for charged particles with $p_T > 0.5\,\text{GeV/c}$ and $|\eta| < 1$ when $P_{T1} > 5$ and $30\,\text{GeV/c}$. The points are $\langle N_{\rm chg}\rangle$ in a $\Delta R = 0.02$ bin. The $P_{T1} > 5\,\text{GeV/c}$ points are Min-Bias data and the $P_{T1} > 30\,\text{GeV/c}$ points are JET20 data. The data are compared with the QCD hard scattering Monte-Carlo predictions of HERWIG, ISAJET, and PYTHIA 6.115. For an average charged jet with $P_{T1} > 5\,\text{GeV/c}$ ($> 30\,\text{GeV/c}$), 80% of the charged particles lie within $R = 0.44$ (0.38) as marked by the arrows.

We can study the radial distribution of charged particles and transverse momentum within the leading jet by examining the distribution of $\langle N_{\rm chg}\rangle$ and $\langle P_T(\text{sum})\rangle$ as a function of the distance in η-ϕ space from the leading jet direction as illustrated in Fig. 7. Fig. 8 and Fig. 9 compare data on the radial multiplicity distribution and the radial transverse momentum distribution, for $P_{T1} > 5\,\text{GeV/c}$ and $30\,\text{GeV/c}$ compared with the QCD hard scattering Monte-Carlo predictions. For an average charged jet with $P_{T1} > 5\,\text{GeV/c}$ ($> 30\,\text{GeV/c}$), 80% of the jet p_T lies within $R = 0.36$ (0.18). Note that because of the nature of QCD fluctuations the average jet size shown in Fig. 6 is not exactly the same as the size of an average jet shown in Fig. 8 and 9. A given charged jet rarely looks like an average charged jet and at low P_{T1} the average jet size is slightly smaller than the size of an average jet.

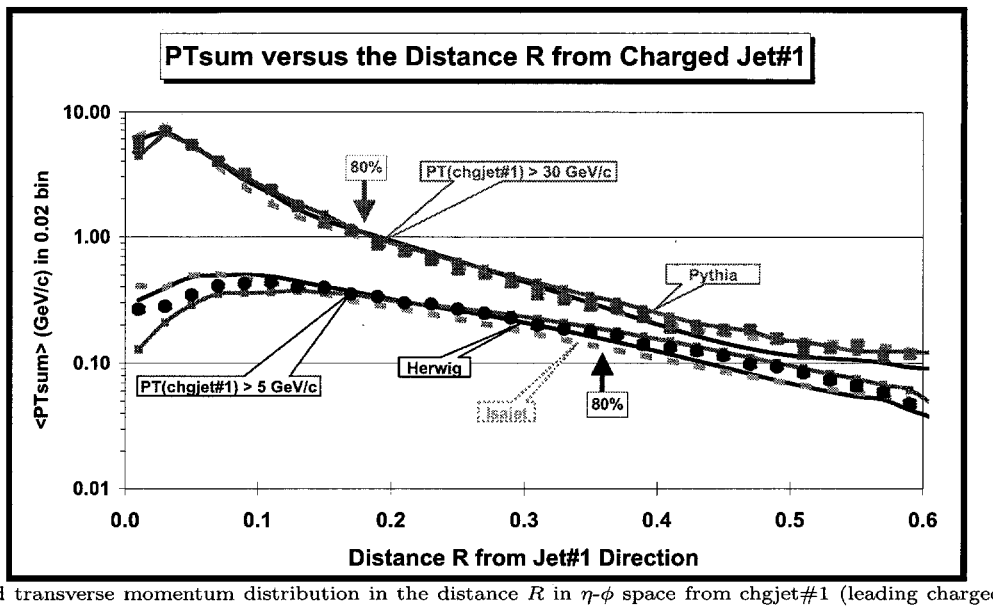

FIG. 9. Charged transverse momentum distribution in the distance R in η-ϕ space from chgjet#1 (leading charged jet) for charged particles with $p_T > 0.5\,\mathrm{GeV/c}$ and $|\eta| < 1$ when $P_{T1} > 5\,\mathrm{GeV/c}$ and $30\,\mathrm{GeV/c}$. The points are $\langle P_T(\mathrm{sum})\rangle$ in a $\Delta R = 0.02$ bin. The $P_{T1} > 5\,\mathrm{GeV/c}$ points are Min-Bias data and the $P_{T1} > 30\,\mathrm{GeV/c}$ points are JET20 data. The data are compared with the QCD hard scattering Monte-Carlo predictions of HERWIG, ISAJET, and PYTHIA 6.115. For an average charged jet with $P_{T1} > 5\,\mathrm{GeV/c}$ ($> 30\,\mathrm{GeV/c}$), 80% of the jet p_T lies within $R = 0.36$ (0.18) as marked by the arrows. (Note the logarithmic scale on the vertical axis.)

D. Momentum Distribution of Charged Particles within Charged Jet#1

We define a charged jet fragmentation function, $F(z)$, which describes the momentum distribution of charged particles within the leading charged particle jet. The function $F(z)$ is the number of charged particles between z and $z + dz$ (i.e., the charged particle number density), where $z = p/P(\mathrm{chgjet\#1})$ is the fraction of the overall charged particle momentum of the jet carried by the charged particle with momentum p. The integral of $F(z)$ over z is the average multiplicity of charged particles within the jet. We refer to this as a fragmentation function, however it is not a true fragmentation function since we are dealing only with charged particle jets. Furthermore, some of the charged particles within the leading jets originate from the underlying event and we can never be sure that we have included all the particles that come from the outgoing high transverse momentum parton. Nevertheless, applying this algorithm to both the data and the Monte-Carlo models allows comparison of the charged particle momentum distribution.

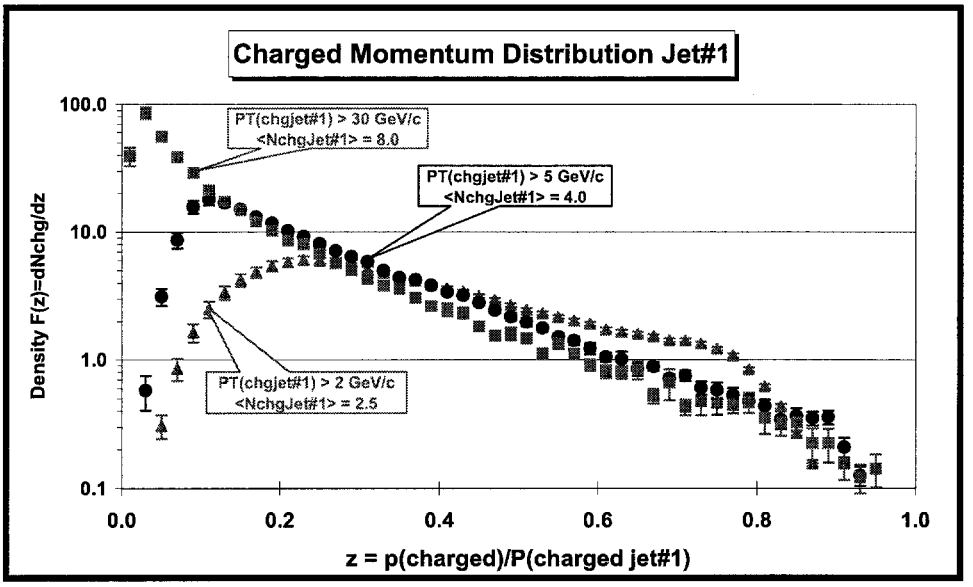

FIG. 10. Momentum distribution of charged particles ($p_T > 0.5\,\mathrm{GeV/c}$, $|\eta| < 1$) within chgjet#1 (leading charged jet). The points are the charged number density, $F(z) = dN_{\mathrm{chg}}/dz$, where $z = p/P(\mathrm{chgjet\#1})$ is the ratio of the charged particle momentum to the charged momentum of chgjet#1. The integral of $F(z)$ is the average number of particles within chgjet#1 (see Fig. 5). The $P_{T1} > 2\,\mathrm{GeV/c}$ and $5\,\mathrm{GeV/c}$ points are Min-Bias data and the $P_{T1} > 30\,\mathrm{GeV/c}$ points are JET20 data. (Note the logarithmic scale on the vertical axis.)

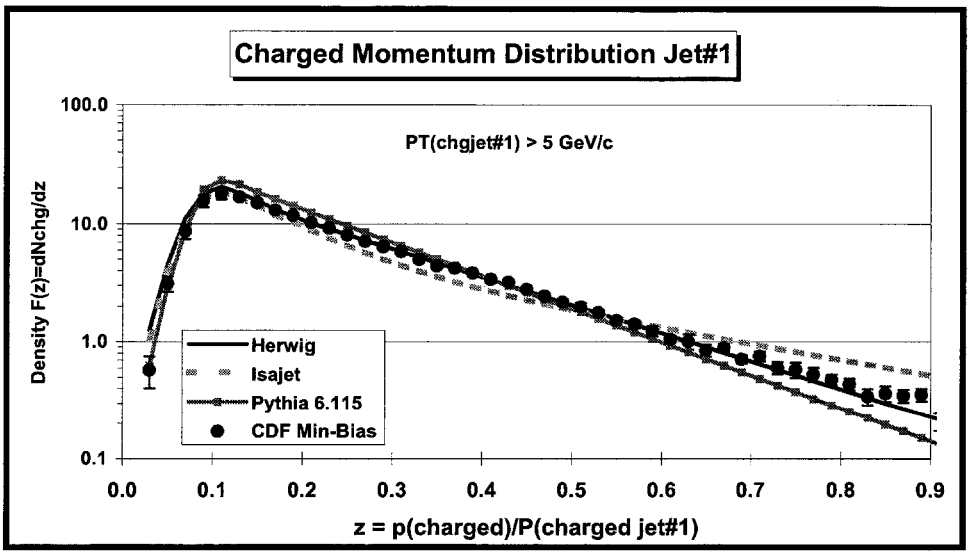

FIG. 11. Data from Fig. 10 on the momentum distribution of charged particles ($p_T > 0.5\,\mathrm{GeV/c}$, $|\eta| < 1$) within chgjet#1 (leading charged jet) for $P_{T1} > 5\,\mathrm{GeV/c}$ compared with the QCD hard scattering Monte-Carlo predictions of HERWIG, ISAJET, and PYTHIA 6.115. The points are the charged number density, $F(z) = dN_{\mathrm{chg}}/dz$, where $z = p/P(\mathrm{chgjet\#1})$ is the ratio of the charged particle momentum to the charged momentum of chgjet#1. (Note the logarithmic scale on the vertical axis.)

Fig. 10 shows the data on $F(z)$ for $P_{T1} > 2\,\mathrm{GeV/c}$,$5\,\mathrm{GeV/c}$, and $30\,\mathrm{GeV/c}$. The data roughly scale for $P_{T1} > 5\,\mathrm{GeV/c}$ and $z > 0.1$, with the growth in multiplicity coming from the soft particles (i.e., low z region). This is exactly the behavior expected from a true fragmentation function. Fig. 11 and Fig. 12 compare data on the $F(z)$ for $P_{T1} > 5$ and $30\,\mathrm{GeV/c}$, respectively, with the QCD hard scattering Monte-Carlo predictions of HERWIG, ISAJET, and PYTHIA.

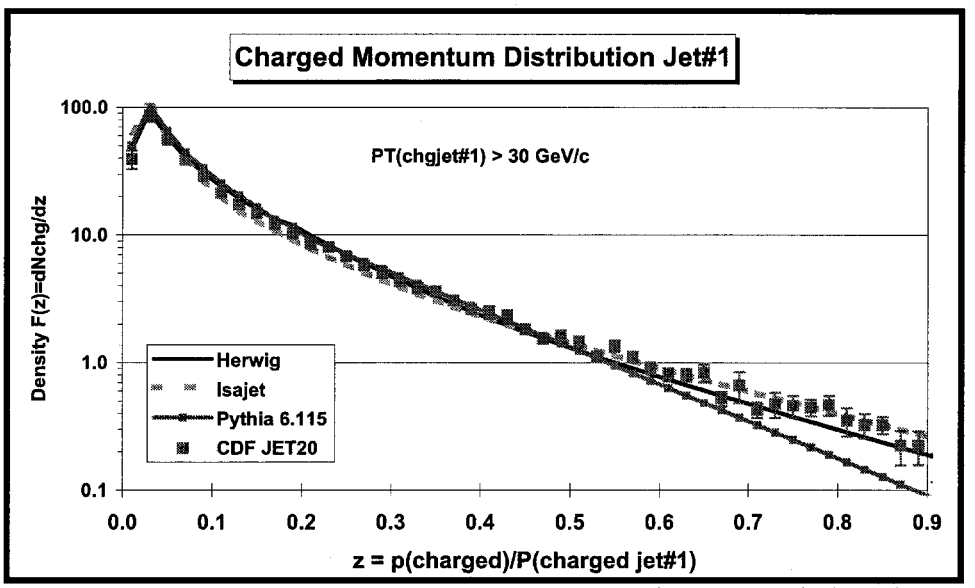

FIG. 12. Data from Fig. 10 on the momentum distribution of charged particles ($p_T > 0.5\,\mathrm{GeV/c}$, $|\eta| < 1$) within chgjet#1 (leading charged jet) for $P_{T1} > 30\,\mathrm{GeV/c}$ compared with the QCD hard scattering Monte-Carlo predictions of HERWIG, ISAJET, and PYTHIA 6.115. The points are the charged number density, $F(z) = dN_{\mathrm{chg}}/dz$, where $z = p/P(\mathrm{chgjet\#1})$ is the ratio of the charged particle momentum to the charged momentum of chgjet#1. (Note the logarithmic scale on the vertical axis.)

The QCD hard scattering models describe quite well the multiplicity distribution of charged particles within the leading jet (Fig. 5), the size of the leading jet (Fig. 6), the radial distribution of charged particles and transverse momentum around the leading jet direction (Fig. 8, Fig. 9), and the momentum distribution of charged particles within the leading jet (Fig. 11, Fig. 12). We now proceed to study the overall event structure as a function of transverse momentum of the leading charged jet.

IV. THE OVERALL EVENT STRUCTURE

In the previous section we studied leading charged jet observables. The QCD Monte-Carlo models did not have to describe correctly the overall event in order to fit these observables. They only had to describe correctly the properties of the leading charged particle jet, and all the models fit the data fairly well (although not perfectly). Now we will study global observables, where to fit the observable the QCD Monte-Carlo models will have to describe correctly the overall event structure.

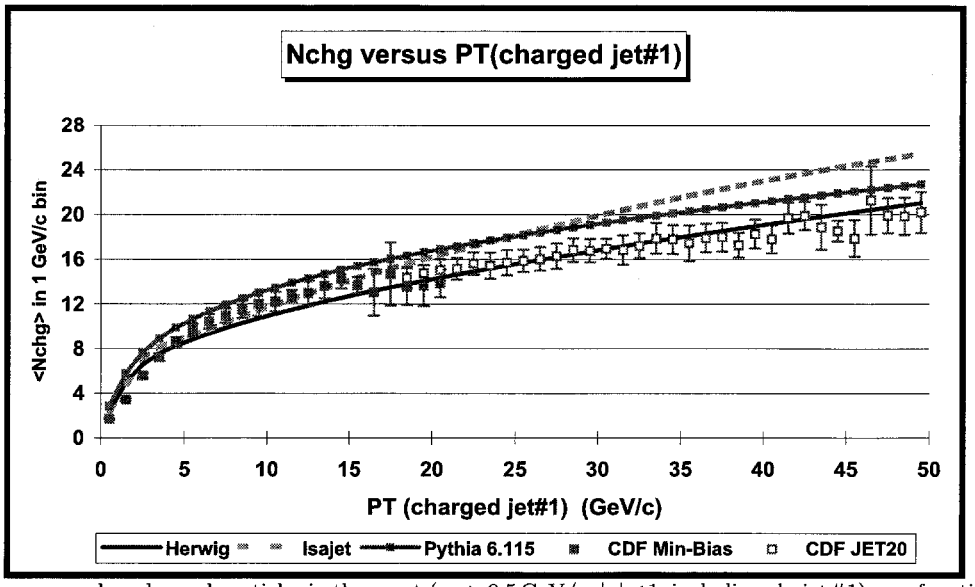

FIG. 13. The average number charged particles in the event ($p_T > 0.5\,\mathrm{GeV/c}$, $|\eta| < 1$, including chgjet#1) as a function of the transverse momentum of the leading charged jet. The solid (open) points are the Min-Bias (JET20) data. The data are compared with the QCD hard scattering Monte-Carlo predictions of HERWIG, ISAJET, and PYTHIA 6.115.

A. Overall Charged Multiplicity versus P_{T1}

Fig. 13 shows the average number of charged particles in the event with $p_T > 0.5\,\mathrm{GeV/c}$ and $|\eta| < 1$ (including chgjet#1) as a function of P_{T1} (leading charged jet) for the Min-Bias and JET20 data. Again the JET20 data connect smoothly to the Min-Bias data and there is a small overlap region where the Min-Bias and JET20 data agree. Fig. 13 shows a sharp rise in the overall charged multiplicity at low P_{T1} and then a more gradual rise at high P_{T1} similar to Fig. 4. We now investigate where these charged particles are located relative to the direction of the leading charged particle jet.

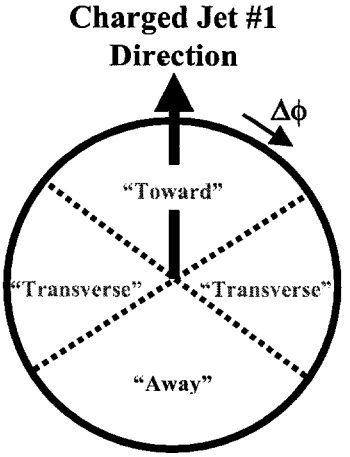

FIG. 14. Illustration of correlations in azimuthal angle $\Delta\phi$ relative to the direction of the leading charged jet in the event, chgjet#1. The angle $\Delta\phi = \phi - \phi_{\text{chgjet\#1}}$ is the relative azimuthal angle between charged particles and the direction of chgjet#1. The region $|\Delta\phi| < 60°$ is referred to as toward chgjet#1 (includes particles in chgjet#1) and the region $|\Delta\phi| > 120°$ is called away from chgjet#1. The transverse to chgjet#1 region is defined by $60° < |\Delta\phi| < 120°$. Each region, toward, transverse, and away covers the same range $|\Delta\eta| \times |\Delta\phi| = 2 \times 120°$.

B. Correlations in $\Delta\phi$ relative to Charged Jet#1

As illustrated in Fig. 14, the angle $\Delta\phi$ is defined to be the relative azimuthal angle between charged particles and the direction of the leading charged particle jet. When we plot $\langle N_{\text{chg}} \rangle$ and $\langle P_T(\text{sum}) \rangle$ as a function of $\Delta\phi$, we include all charged particles with $p_T > 0.5\,\text{GeV/c}$ and $|\eta| < 1$(including those in chgjet#1). Fig. 15 and Fig. 16 shows the data on the charged multiplicity distribution and transverse momentum distribution, respectively, in the azimuthal angle $\Delta\phi$ relative to the leading charged particle jet for $P_{T1} > 2\,\text{GeV/c}$, $5\,\text{GeV/c}$, and $30\,\text{GeV/c}$.

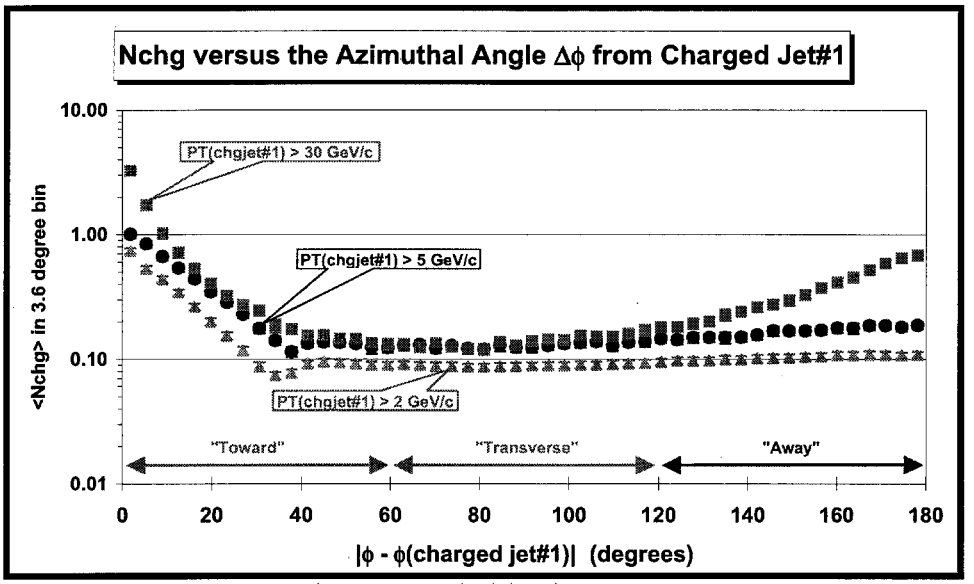

FIG. 15. Average number of charged particles ($p_T > 0.5\,\text{GeV/c}$, $|\eta| < 1$) as a function of the relative azimuthal angle, $\Delta\phi$, between the particle and chgjet#1 (leading charged jet) for $P_{T1} > 2\,\text{GeV/c}$, $5\,\text{GeV/c}$, and $30\,\text{GeV/c}$. Each point corresponds to the $\langle N_{\text{chg}} \rangle$ in a 3.6° bin. The $P_{T1} > 2\,\text{GeV/c}$ and $5\,\text{GeV/c}$ points are the Min-Bias data and the $P_{T1} > 30\,\text{GeV/c}$ points are JET20 data. The toward, transverse, and away regions are defined in Fig. 14. (Note the logarithmic scale on the vertical axis.)

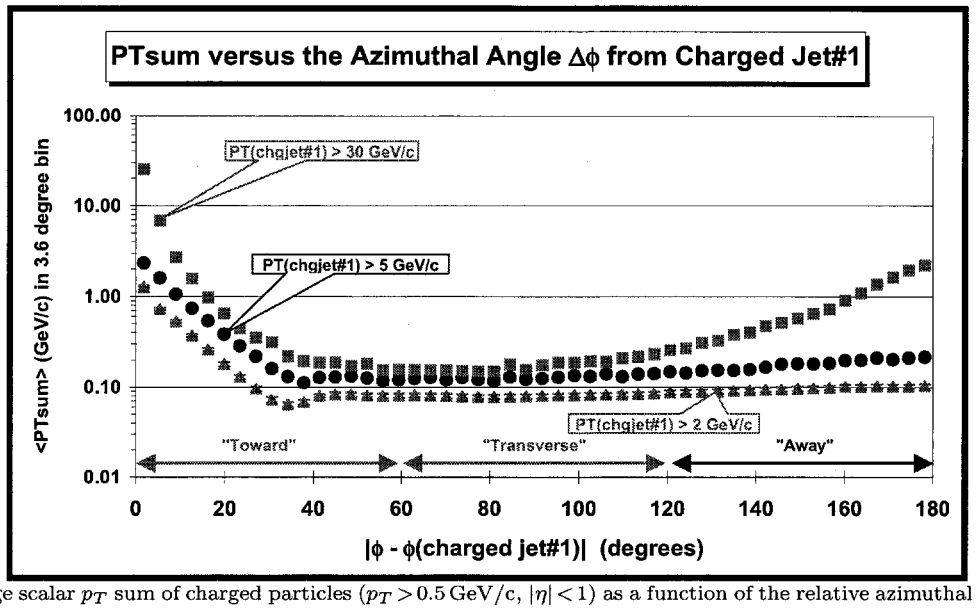

FIG. 16. Average scalar p_T sum of charged particles ($p_T > 0.5\,\mathrm{GeV/c}$, $|\eta| < 1$) as a function of the relative azimuthal angle, $\Delta\phi$, between the particle and chgjet#1 (leading charged jet) for $P_{T1} > 2\,\mathrm{GeV/c}$, $5\,\mathrm{GeV/c}$, and $30\,\mathrm{GeV/c}$. Each point corresponds to the $\langle P_T(\mathrm{sum})\rangle$ in a 3.6° bin. The $P_{T1} > 2\,\mathrm{GeV/c}$ and $5\,\mathrm{GeV/c}$ points are the Min-Bias data and the $P_{T1} > 30\,\mathrm{GeV/c}$ points are JET20 data. The toward, transverse, and away regions are defined in Fig. 14. (Note the logarithmic scale on the vertical axis.)

Fig. 17 and Fig. 18 compare the data on the azimuthal distribution of charged multiplicity and transverse momentum relative to the leading charged particle jet with the QCD hard scattering Monte- Carlo predictions of HERWIG, ISAJET, and PYTHIA for $P_{T1} > 5\,\mathrm{GeV/c}$ and Fig. 19 and Fig. 20 for $P_{T1} > 30\,\mathrm{GeV/c}$. Here one sees differences in the QCD Monte-Carlo models and they do not agree as well with these global observables as they did with the leading jet observables. The kink in data and the Monte-Carlo predictions around $\Delta\phi = 40°$ arises from the cone size choice of $R = 0.7$ which we used in defining the charged particle jets.

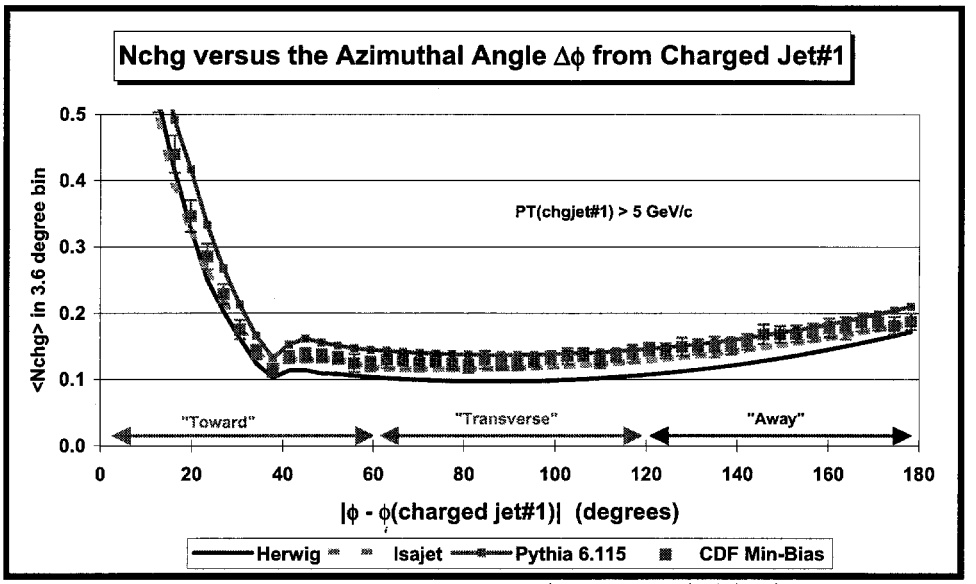

FIG. 17. Data from Fig. 15 on the average number of charged particles ($p_T > 0.5\,\mathrm{GeV/c}$, $|\eta| < 1$) as a function of the relative azimuthal angle, $\Delta\phi$, between the particle and chgjet#1 (leading charged jet) for $P_{T1} > 5\,\mathrm{GeV/c}$ compared to QCD hard scattering Monte-Carlo predictions of HERWIG , ISAJET, and PYTHIA 6.115. Each point corresponds to the $\langle N_{\mathrm{chg}}\rangle$ in a 3.6° bin. The toward, transverse, and away regions are defined in Fig. 14.

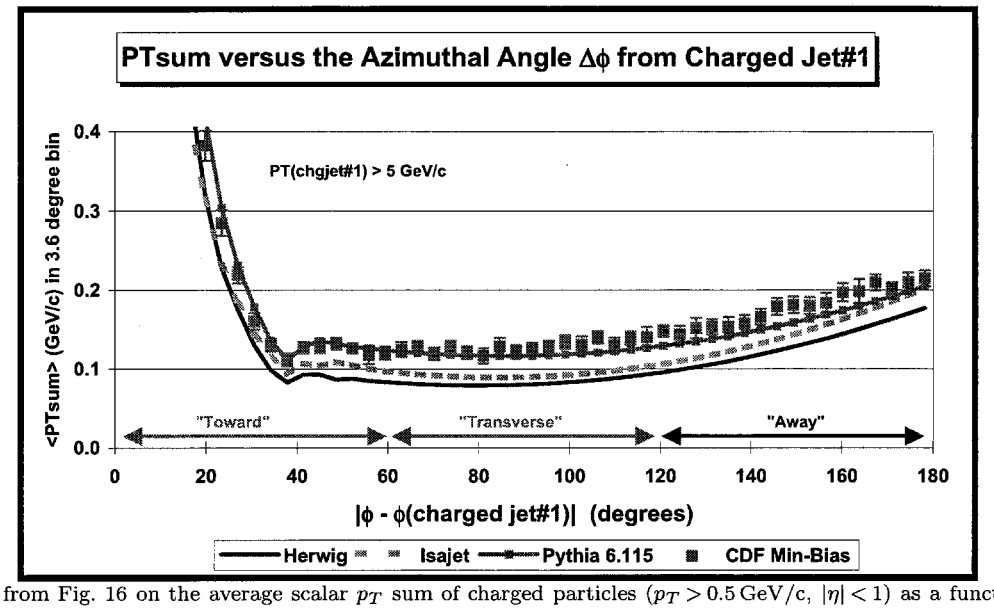

FIG. 18. Data from Fig. 16 on the average scalar p_T sum of charged particles ($p_T > 0.5\,\mathrm{GeV/c}$, $|\eta| < 1$) as a function of the relative azimuthal angle, $\Delta\phi$, between the particle and chgjet#1 (leading charged jet) for $P_{T1} > 5\,\mathrm{GeV/c}$ compared to QCD hard scattering Monte-Carlo predictions of HERWIG, ISAJET, and PYTHIA 6.115. Each point corresponds to the $\langle P_T(\mathrm{sum})\rangle$ in a 3.6° bin. The toward, transverse, and away regions are defined in Fig. 14.

In Fig. 15 and Fig. 16 we have labeled the region $|\phi - \phi_{\mathrm{chgjet\#1}}| < 60°$ as toward chgjet#1 and the region $|\phi - \phi_{\mathrm{chgjet\#1}}| > 120°$ as away from chgjet#1. The transverse region is defined by $60° < |\phi - \phi_{\mathrm{jet\#1}}| < 120°$. As illustrated in Fig. 14, each region, toward, transverse, and away covers the same range $|\Delta\eta| \times |\Delta\phi| = 2 \times 120°$. The toward region includes the particles from chgjet#1 as well as a few particles from the underlying event. As we will see, the transverse region is very sensitive to the underlying event since it is roughly normal to the plane of the 2-to-2 hard scattering. The away region is a mixture of the underlying event and the away-side hard scattering jet. Fig. 15 and Fig. 16 show a rapid growth in the toward and away region as P_{T1} increases.

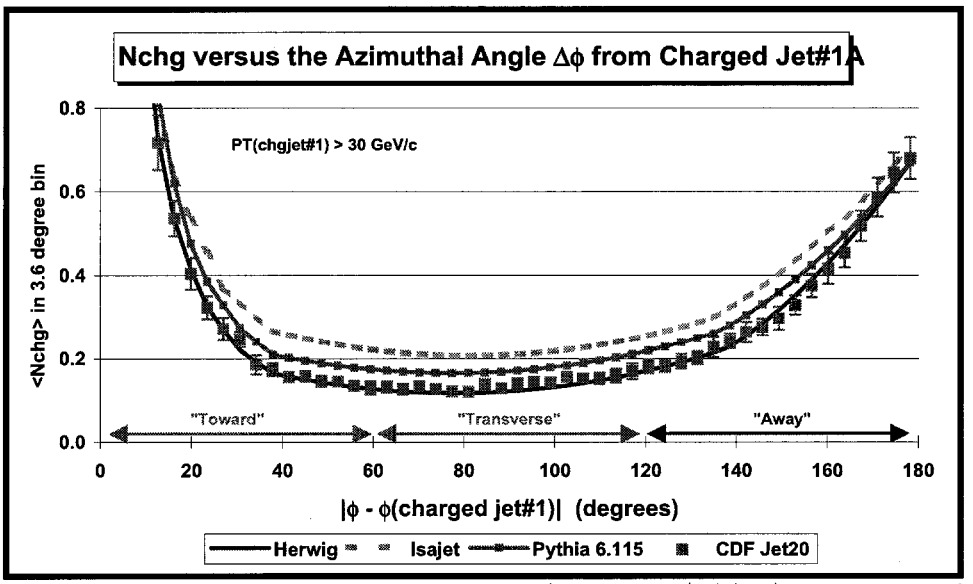

FIG. 19. Data from Fig. 15 on the average number of charged particles ($p_T > 0.5\,\mathrm{GeV/c}$, $|\eta| < 1$) as a function of the relative azimuthal angle, $\Delta\phi$, between the particle and chgjet#1 (leading charged jet) for $P_{T1} > 30\,\mathrm{GeV/c}$ compared to QCD hard scattering Monte-Carlo predictions of HERWIG , ISAJET, and PYTHIA 6.115. Each point corresponds to the $\langle N_{\mathrm{chg}}\rangle$ in a 3.6° bin. The toward, transverse, and away regions are defined in Fig. 14.

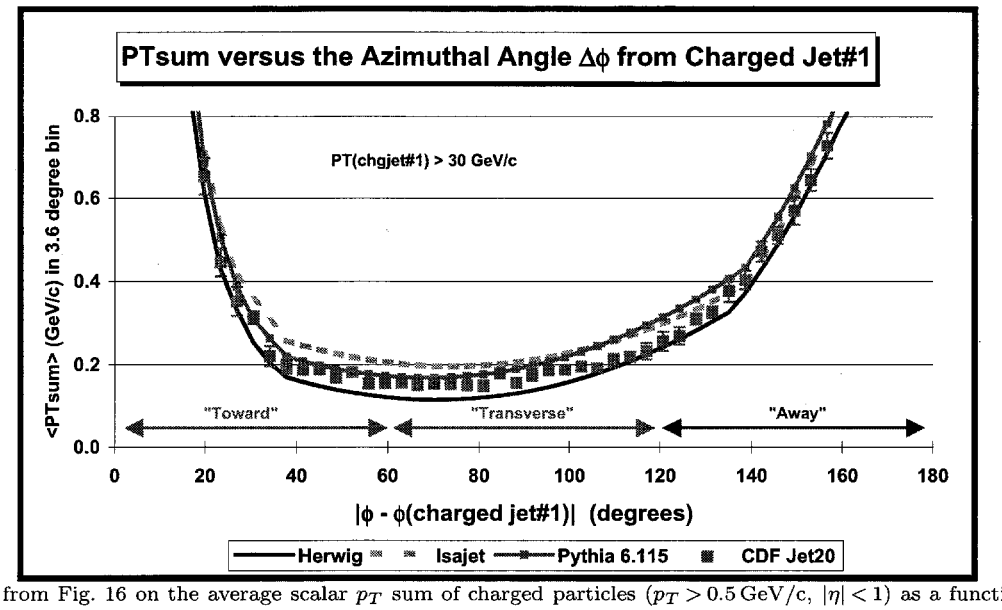

FIG. 20. Data from Fig. 16 on the average scalar p_T sum of charged particles ($p_T > 0.5\,\mathrm{GeV/c}$, $|\eta| < 1$) as a function of the relative azimuthal angle, $\Delta\phi$, between the particle and chgjet#1 (leading charged jet) for $P_{T1} > 30\,\mathrm{GeV/c}$ compared to QCD hard scattering Monte-Carlo predictions of HERWIG, ISAJET, and PYTHIA 6.115. Each point corresponds to the $\langle P_T(\mathrm{sum})\rangle$ in a 3.6° bin. The toward, transverse, and away regions are defined in Fig. 14.

Fig. 21 shows the data on the average number of charged particles ($p_T > 0.5\,\mathrm{GeV/c}$ and $|\eta| < 1$) as a function of P_{T1} for the three regions. Each point corresponds to the toward, transverse, or away $\langle N_{\mathrm{chg}}\rangle$ in a $1\,\mathrm{GeV/c}$ bin. The solid points are Min-Bias data and the open points are JET20 data. The data in Fig. 21 define the average event shape. For example, for a proton-antiproton collider event at 1.8 TeV with $P_{T1} = 20\,\mathrm{GeV/c}$ there are, on the average, 8.7 charged particles toward chgjet#1 (including the particles in chgjet#1), 2.5 transverse to chgjet#1, and 4.9 away from chgjet#1. Of course, $\langle N_{\mathrm{chg}}\rangle$ in all three regions is forced to go to zero as P_{T1} goes to zero. If the leading charged particle jet has no particles then there are no charged particles anywhere.

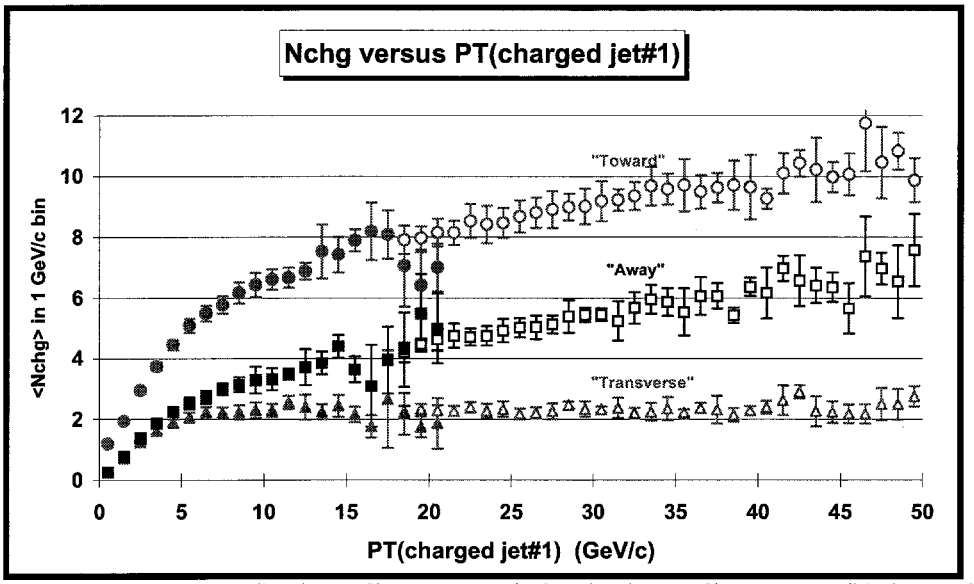

FIG. 21. The average number of toward ($|\Delta\phi| < 60°$), transverse ($60° < |\Delta\phi| < 120°$), and away ($|\Delta\phi| > 120°$) charged particles ($p_T > 0.5\,\mathrm{GeV/c}$, $|\eta| < 1$, including chgjet#1) as a function of the transverse momentum of the leading charged jet. Each point corresponds to the $\langle N_{\mathrm{chg}}\rangle$ in a $1\,\mathrm{GeV/c}$ bin. The solid (open) points are the Min-Bias (JET20) data. The errors on the (uncorrected) data include both statistical and correlated systematic uncertainties. The toward, transverse, and away regions are illustrated in Fig. 14 and labeled in Fig. 15.

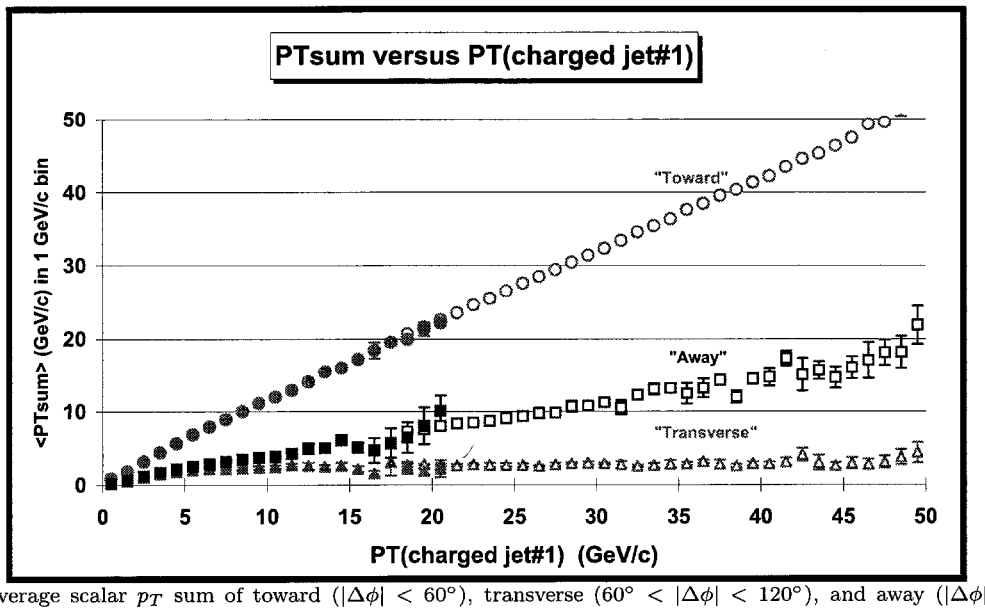

FIG. 22. The average scalar p_T sum of toward ($|\Delta\phi| < 60°$), transverse ($60° < |\Delta\phi| < 120°$), and away ($|\Delta\phi| > 120°$) charged particles ($p_T > 0.5\,\mathrm{GeV/c}$, $|\eta| < 1$, including chgjet#1) as a function of the transverse momentum of the leading charged jet. Each point corresponds to the $\langle P_T(\mathrm{sum})\rangle$ in a 1 GeV/c bin. The solid (open) points are the Min-Bias (JET20) data. The errors on the (uncorrected) data include both statistical and correlated systematic uncertainties. The toward, transverse, and away regions are illustrated in Fig. 14 and labeled in Fig. 16.

Fig. 22 shows the data on the average scalar p_T sum of charged particles ($p_T > 0.5\,\mathrm{GeV/c}$ and $|\eta| < 1$) as a function of P_{T1} for the three regions. Each point corresponds to the toward, transverse, or away $\langle P_T(\mathrm{sum})\rangle$ in a 1 GeV/c bin. We will now examine more closely these three regions.

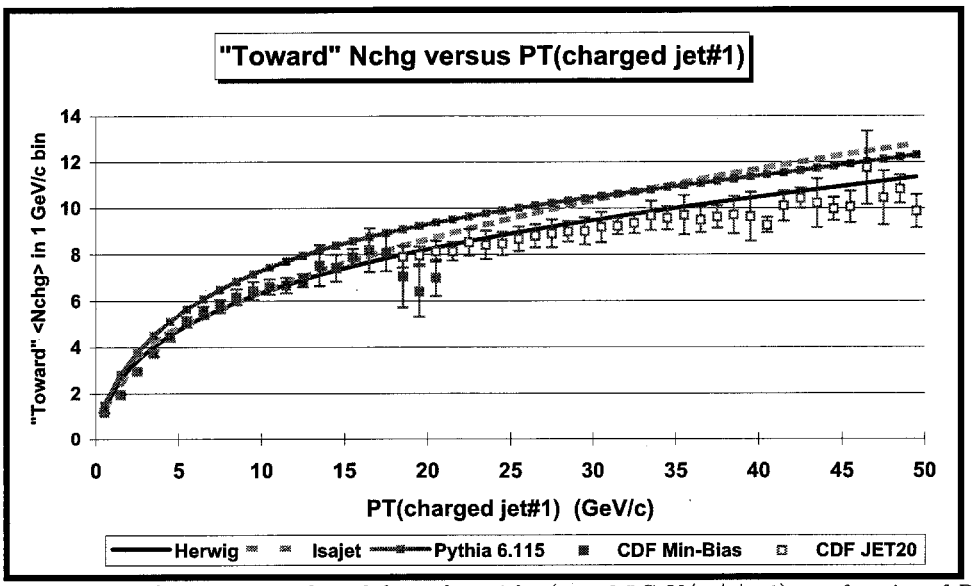

FIG. 23. Data from Fig. 21 on the average number of charged particles ($p_T > 0.5\,\mathrm{GeV/c}$, $|\eta| < 1$) as a function of P_{T1} (leading charged jet) for the toward region defined in Fig. 14 compared with the QCD hard scattering Monte-Carlo predictions of HERWIG, ISAJET, and PYTHIA 6.115. The solid (open) points are the Min-Bias (JET20) data. Each point corresponds to the toward $\langle N_{\mathrm{chg}}\rangle$ in a 1 GeV/c bin.

C. The Toward and Away Region versus P_{T1}

Fig. 23 shows the data from Fig. 21 on the average number of toward region charged particles compared with the QCD hard scattering Monte-Carlo predictions of HERWIG, ISAJET, and PYTHIA. This plot is very similar to the average number of charged particles within the leading jet shown in Fig. 4. At $P_{T1} = 20\,\mathrm{GeV/c}$ the toward region

contains, on the average, about 8.7 charged particles with about 6.9 of these charged particles belonging to chgjet#1. As expected the toward region is dominated by the leading charged particle jet. This is seen clearly in Fig. 24 where the predictions of ISAJET for the toward region are divided into three categories: charged particles that arise from the break-up of the beam particles (beam-beam remnants), charged particles that arise from initial-state radiation, and charged particles that result from the outgoing jets plus final-state radiation. For P_{T1} values below 5 GeV/c the toward region charged multiplicity arises mostly from the beam-beam remnants, but as P_{T1} increases the contribution from the outgoing jets plus final state-radiation quickly begins to dominate. The bump in the beam-beam remnant contribution at low P_{T1} is caused by leading jets composed almost entirely from the remnants.

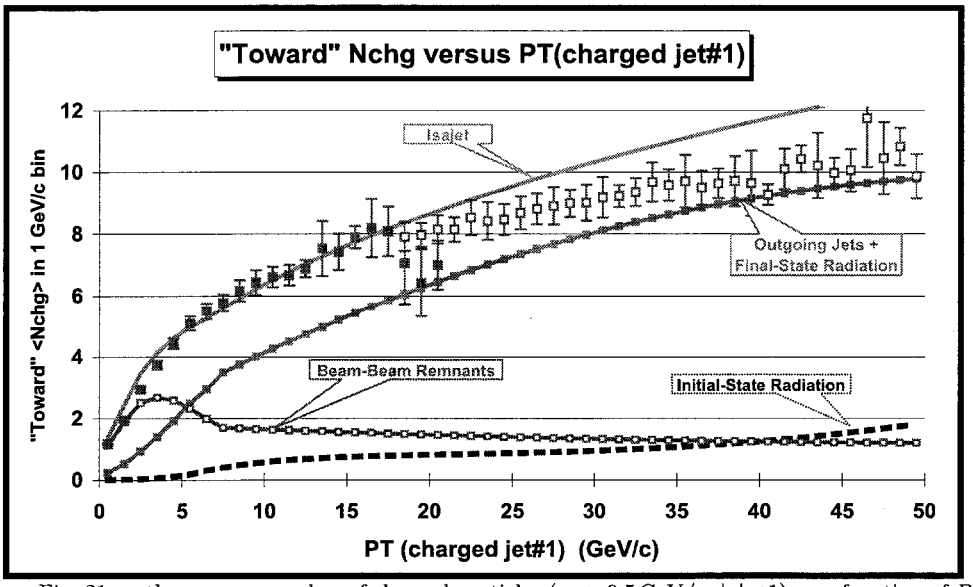

FIG. 24. Data from Fig. 21 on the average number of charged particles ($p_T > 0.5$ GeV/c, $|\eta| < 1$) as a function of P_{T1} (leading charged jet) for the toward region defined in Fig. 14 compared with the QCD hard scattering Monte-Carlo predictions of ISAJET. The predictions of ISAJET are divided into three categories: charged particles that arise from the break-up of the beam particles (beam-beam remnants), charged particles that arise from initial-state radiation, and charged particles that result from the outgoing jets plus final-state radiation (see Fig. 1). The solid (open) points are the Min-Bias (JET20) data.

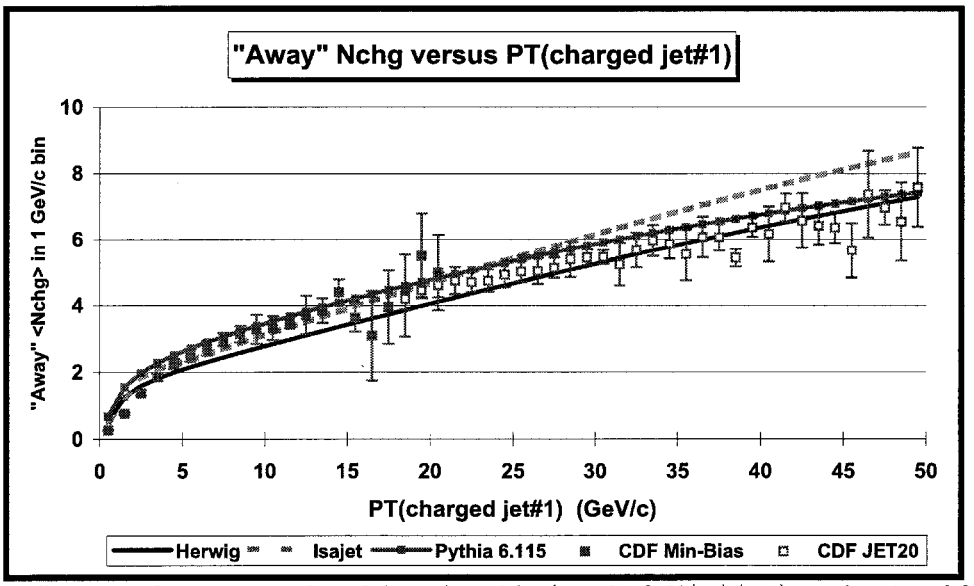

FIG. 25. Data from Fig. 21 on the average number of charged particles ($p_T > 0.5$ GeV/c, $|\eta| < 1$) as a function of P_{T1} (leading charged jet) for the away region defined in Fig. 14 compared with the QCD hard scattering Monte-Carlo predictions of HERWIG, ISAJET, and PYTHIA 6.115. The solid (open) points are the Min-Bias (JET20) data. Each point corresponds to the away $\langle N_{\rm chg} \rangle$ in a 1 GeV/c bin.

Fig. 25 shows the data from Fig. 21 on the average number of away region charged particles compared with the QCD hard scattering Monte-Carlo predictions of HERWIG, ISAJET, and PYTHIA. In Fig. 26 the data from Fig. 22 on the average scalar p_T sum in the away region is compared to the QCD Monte-Carlo predictions. The away region is a mixture of the underlying event and the away-side outgoing hard scattering jet. This can be seen in Fig. 27 where the predictions of ISAJET for the away region are divided into three categories: beam-beam remnants, initial-state radiation, and outgoing jets plus final-state radiation. Here the underlying event plays a more important role since the away-side outgoing hard scattering jet is sometimes outside the region $|\eta| < 1$. For the toward region the contribution from the outgoing jets plus final state-radiation dominates for P_{T1} values above about 5 GeV/c, whereas for the away region this does not occur until around 20 GeV/c.

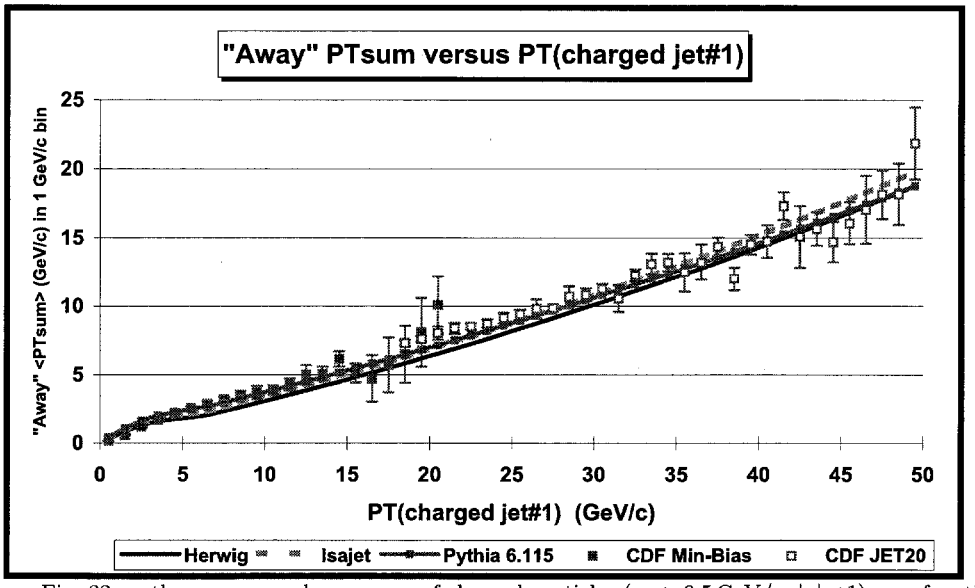

FIG. 26. Data from Fig. 22 on the average scalar p_T sum of charged particles ($p_T > 0.5$ GeV/c, $|\eta| < 1$) as a function of P_{T1} (leading charged jet) for the away region defined in Fig. 14 compared with the QCD hard scattering Monte-Carlo predictions of HERWIG, ISAJET, and PYTHIA 6.115. The solid (open) points are the Min-Bias (JET20) data. Each point corresponds to the away $\langle P_T(\text{sum})\rangle$ in a 1 GeV/c bin.

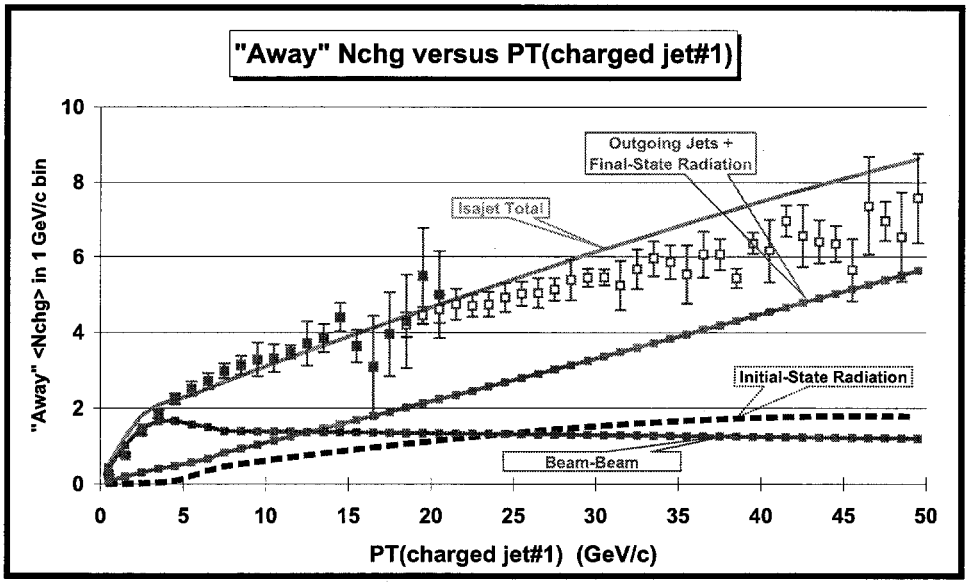

FIG. 27. Data from Fig. 21 on the average number of charged particles ($p_T > 0.5\,\mathrm{GeV/c}$, $|\eta| < 1$) as a function of P_{T1} (leading charged jet) for the away region defined in Fig. 14 compared with the QCD hard scattering Monte-Carlo predictions of ISAJET. The predictions of ISAJET are divided into three categories: charged particles that arise from the break-up of the beam particles (beam-beam remnants), charged particles that arise from initial-state radiation, and charged particles that result from the outgoing jets plus final-state radiation (see Fig. 1). The solid (open) points are the Min-Bias (JET20) data.

Both the toward and away regions are described fairly well by the QCD hard scattering Monte-Carlo models. These regions are dominated by the outgoing hard scattering jets and as we saw in Section III the Monte-Carlo models describe the leading outgoing jets fairly accurately. We will now study the transverse region which is dominated by the underlying event.

V. THE TRANSVERSE REGION AND THE UNDERLYING EVENT

The transverse region in Fig. 14 is roughly normal to the plane of the 2-to-2 hard scattering and as can be seen in Fig. 21 contains, on the average, considerably fewer charged particles than the toward and away region. However, there is a lot more activity in the transverse region than one might naively expect. If we suppose that the transverse multiplicity is uniform in azimuthal angle ϕ and pseudo-rapidity η, the observed 2.3 charged particles at $P_{T1} = 20\,\mathrm{GeV/c}$ translates into 3.8 charged particles per unit pseudo-rapidity with $p_T > 0.5\,\mathrm{GeV/c}$ (multiply by 3 to get 360°, divide by 2 for the two units of pseudo-rapidity covered in this analysis, multiply by 1.09 to correct for the track finding efficiency). We know that if we include all $p_T > 50\,\mathrm{MeV}$ that there are, on the average, about four charged particles per unit rapidity in a soft proton-antiproton collision at 1.8 TeV [6]. The data in Fig. 21 imply that in the underlying event of a hard scattering there are, on the average, about 3.8 charged particles per unit rapidity with $p_T > 0.5\,\mathrm{GeV/c}$. Extrapolating to low p_T assuming the form e^{-2p_T} (which roughly fits our data) implies that there are roughly 10 charged particles per unit pseudo-rapidity with $p_T > 0$ in the underlying event (factor of e). Since we include only those charged particles with $p_T > 0.5\,\mathrm{GeV/c}$, we cannot accurately extrapolate to low p_T, however, it is clear that the underlying event has a charged particle density that is at least a factor of two larger than the four charged particles per unit rapidity seen in soft proton-antiproton collisions at this energy. Fig. 21 shows that the average number of charged particles in the transverse region doubles in going from $P_{T1} = 1.5\,\mathrm{GeV/c}$ to $2.5\,\mathrm{GeV/c}$ and then forms an approximately constant plateau for $P_{T1} > 5\,\mathrm{GeV/c}$.

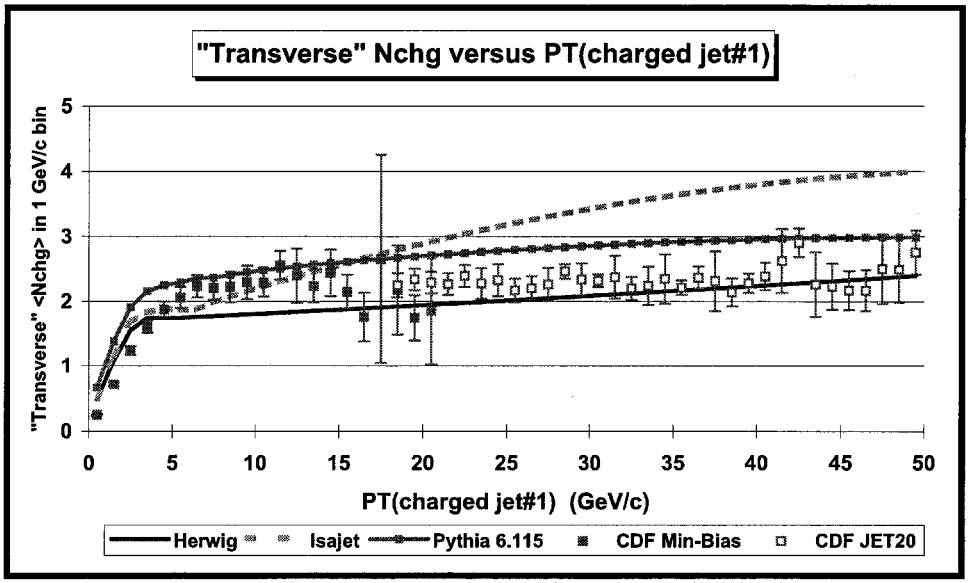

FIG. 28. Data from Fig. 21 on the average number of charged particles ($p_T > 0.5\,\mathrm{GeV/c}$, $|\eta| < 1$) as a function of P_{T1} (leading charged jet) for the transverse region defined in Fig. 14 compared with the QCD hard scattering Monte-Carlo predictions of HERWIG, ISAJET, and PYTHIA 6.115. The solid (open) points are the Min-Bias (JET20) data. Each point corresponds to the transverse $\langle N_{\mathrm{chg}} \rangle$ in a 1 GeV/c bin.

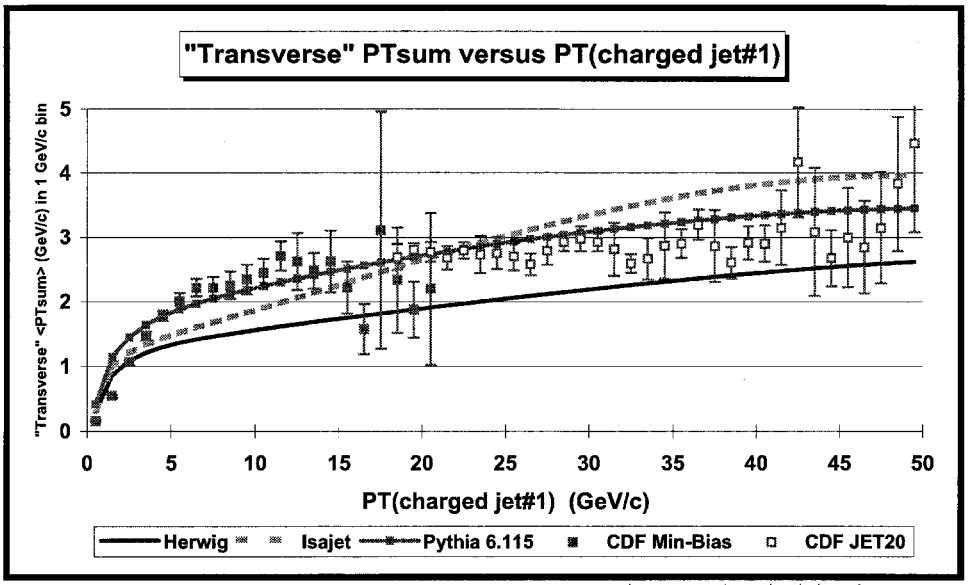

FIG. 29. Data from Fig. 22 on the average scalar p_T sum of charged particles ($p_T > 0.5\,\mathrm{GeV/c}$, $|\eta| < 1$) as a function of P_{T1} (leading charged jet) for the transverse region defined in Fig. 14 compared with the QCD hard scattering Monte-Carlo predictions of HERWIG, ISAJET, and PYTHIA 6.115. The solid (open) points are the Min-Bias (JET20) data. Each point corresponds to the transverse $\langle P_T(\mathrm{sum})\rangle$ in a 1 GeV/c bin.

A. Transverse N_{chg} and $P_T(\mathrm{sum})$ versus P_{T1}

Fig. 28 and Fig. 29 compare the transverse $\langle N_{\mathrm{chg}}\rangle$ and the transverse $\langle P_T(\mathrm{sum})\rangle$, respectively, with the QCD hard scattering Monte-Carlo predictions of HERWIG, ISAJET, and PYTHIA. Fig. 30 and Fig. 31 compare the transverse $\langle N_{\mathrm{chg}}\rangle$ and the transverse $\langle P_T(\mathrm{sum})\rangle$, respectively, with three versions of PYTHIA (6.115, 6.125, and no multiple scattering, see Table 2). PYTHIA with no multiple parton scattering does not have enough activity in the underlying event. PYTHIA 6.115 fits the transverse $\langle N_{\mathrm{chg}}\rangle$ the best, but overshoots slightly the toward $\langle N_{\mathrm{chg}}\rangle$ in Fig. 23. ISAJET has a lot of activity in the underlying event, but gives the wrong P_{T1} dependence. Instead of a plateau, ISAJET predicts a rising transverse $\langle N_{\mathrm{chg}}\rangle$ and gives too much activity at large P_{T1} values. HERWIG does not have enough transverse $\langle P_T(\mathrm{sum})\rangle$.

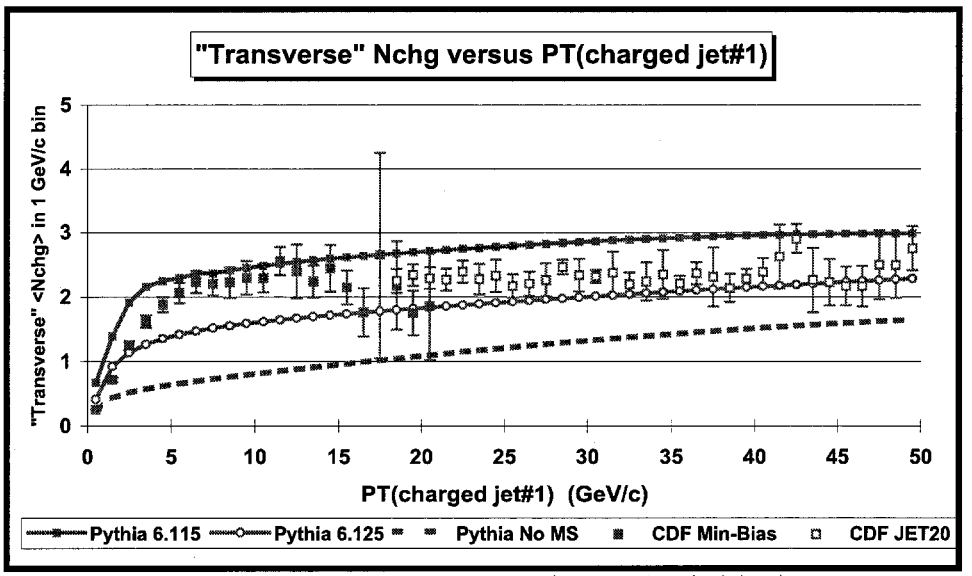

FIG. 30. Data from Fig. 21 on the average number of charged particles ($p_T > 0.5\,\mathrm{GeV/c}$, $|\eta| < 1$) as a function of P_{T1} (leading charged jet) for the transverse region defined in Fig. 14 compared with the QCD hard scattering Monte-Carlo predictions of PYTHIA 6.115, PYTHIA 6.125, and PYTHIA 6.115 with no multiple parton scattering (No MS). The solid (open) points are the Min-Bias (JET20) data. Each point corresponds to the transverse $\langle N_{\mathrm{chg}}\rangle$ in a 1 GeV/c bin.

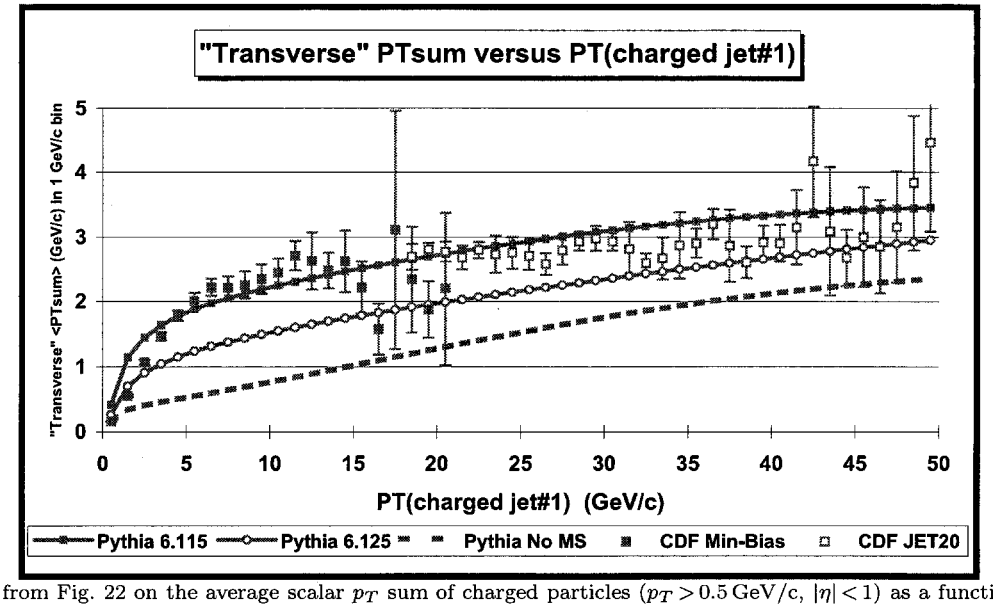

FIG. 31. Data from Fig. 22 on the average scalar p_T sum of charged particles ($p_T > 0.5\,\mathrm{GeV/c}$, $|\eta| < 1$) as a function of P_{T1} (leading charged jet) for the transverse region defined in Fig. 14 compared with the QCD hard scattering Monte-Carlo predictions of PYTHIA 6.115, PYTHIA 6.125, and PYTHIA with no multiple parton scattering (No MS). The solid (open) points are the Min-Bias (JET20) data. Each point corresponds to the transverse $\langle P_T(\mathrm{sum})\rangle$ in a 1 GeV/c bin.

We expect the transverse region to be composed predominately from particles that arise from the break-up of the beam particles and from initial-state radiation. This is clearly the case as can be seen in Fig. 32 where the predictions of ISAJET for the transverse region are divided into three categories: beam-beam remnants, initial-state radiation, and outgoing jets plus final-state radiation. It is interesting to see that it is the beam-beam remnants that are producing the approximately constant plateau. The contributions from initial-state radiation and from the outgoing hard scattering jets both increase as P_{T1} increases. In fact, for ISAJET it is the sharp rise in the initial-state radiation component that is causing the disagreement with the data for $P_{T1} > 20\,\mathrm{GeV/c}$.

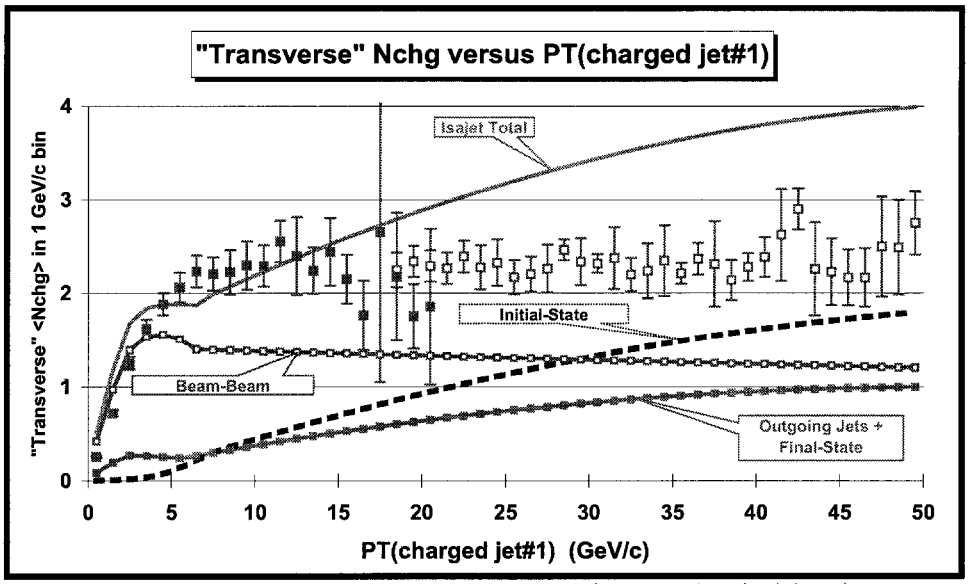

FIG. 32. Data from Fig. 21 on the average number of charged particles ($p_T > 0.5\,\mathrm{GeV/c}$, $|\eta| < 1$) as a function of P_{T1} (leading charged jet) for the transverse region defined in Fig. 14 compared with the QCD hard scattering Monte-Carlo predictions of ISAJET. The predictions of ISAJET are divided into three categories: charged particles that arise from the break-up of the beam particles (beam-beam remnants), charged particles that arise from initial-state radiation, and charged particles that result from the outgoing jets plus final-state radiation (see Fig. 1). The solid (open) points are the Min-Bias (JET20) data.

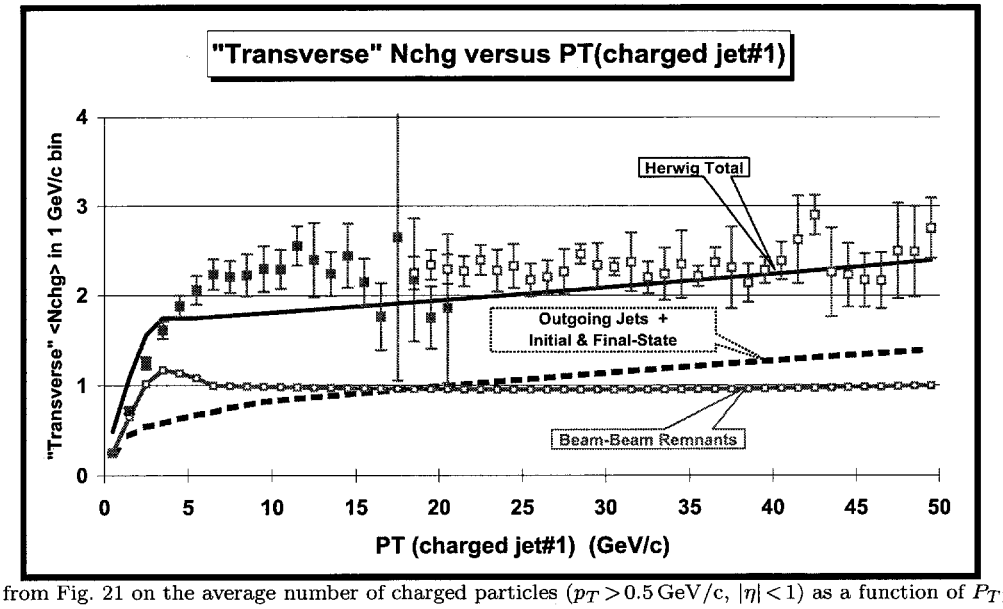

FIG. 33. Data from Fig. 21 on the average number of charged particles ($p_T > 0.5\,\mathrm{GeV/c}$, $|\eta| < 1$) as a function of P_{T1} (leading charged jet) for the transverse region defined in Fig. 14 compared with the QCD hard scattering Monte-Carlo predictions of HERWIG. The predictions of HERWIG are divided into two categories: charged particles that arise from the break-up of the beam particles (beam-beam remnants), and charged particles that result from the outgoing jets plus initial and final-state radiation (hard scattering component) (see Fig. 1). The solid (open) points are the Min-Bias (JET20) data.

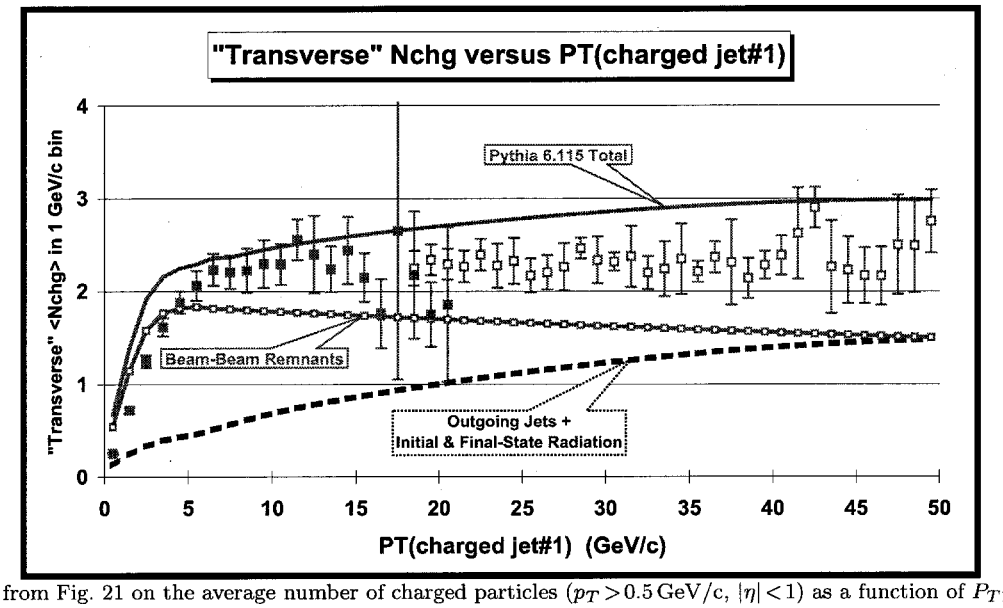

FIG. 34. Data from Fig. 21 on the average number of charged particles ($p_T > 0.5\,\mathrm{GeV/c}$, $|\eta| < 1$) as a function of P_{T1} (leading charged jet) for the transverse region defined in Fig. 14 compared with the QCD hard scattering Monte-Carlo predictions of PYTHIA 6.115. The predictions of PYTHIA are divided into two categories: charged particles that arise from the break-up of the beam particles (beam-beam remnants), and charged particles that result from the outgoing jets plus initial and final-state radiation (hard scattering component). For PYTHIA the beam-beam remnants include contributions from multiple parton scattering (see Fig. 2). The solid (open) points are the Min-Bias (JET20) data.

As we explained in Section II, for PYTHIA it makes no sense to distinguish particles that arise from initial-state radiation from those that arise from final-state radiation, but one can separate the hard scattering component from the beam-beam remnants. Also, for PYTHIA the beam-beam remnants include contributions from multiple parton scattering as illustrated in Fig. 2. Fig. 33 and Fig. 34 compare the transverse $\langle N_{\mathrm{chg}} \rangle$ with the QCD hard scattering Monte-Carlo predictions of HERWIG and PYTHIA 6.115, respectively. Here the predictions are divided into two categories: charged particles that arise from the break-up of the beam particles (beam-beam remnants), and charged

particles that result from the outgoing jets plus initial and final-state radiation (hard scattering component). As was the case with ISAJET the beam-beam remnants form the approximately constant plateau and the hard scattering components increase as P_{T1} increases. However, the hard scattering component of HERWIG and PYTHIA does not rise nearly as fast as the hard scattering component of ISAJET. This can be seen clearly in Fig. 35 where we compare directly the hard scattering component (outgoing jets plus initial and final-state radiation) of the transverse $\langle N_{\rm chg} \rangle$ from ISAJET, HERWIG, and PYTHIA 6.115. PYTHIA and HERWIG are similar and rise gently as P_{T1} increases, whereas ISAJET produces a much sharper increase as P_{T1} increases.

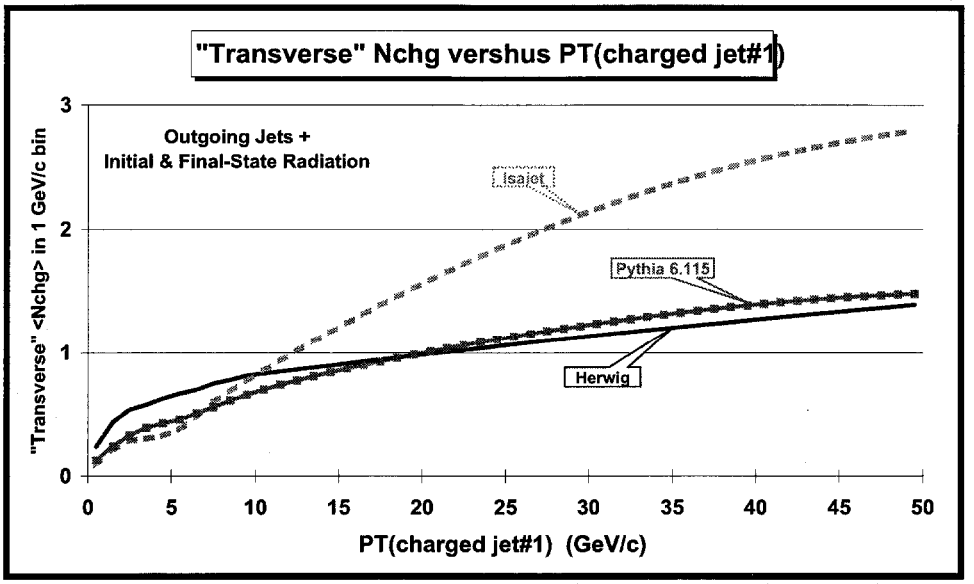

FIG. 35. QCD hard scattering Monte-Carlo predictions from HERWIG, ISAJET, and PYTHIA 6.115 of the average number of charged particles ($p_T > 0.5\,\mathrm{GeV/c}$, $|\eta| < 1$) as a function of P_{T1} (leading charged jet) for the transverse region defined in Fig. 14 arising from the outgoing jets plus initial and finial-state radiation (hard scattering component).

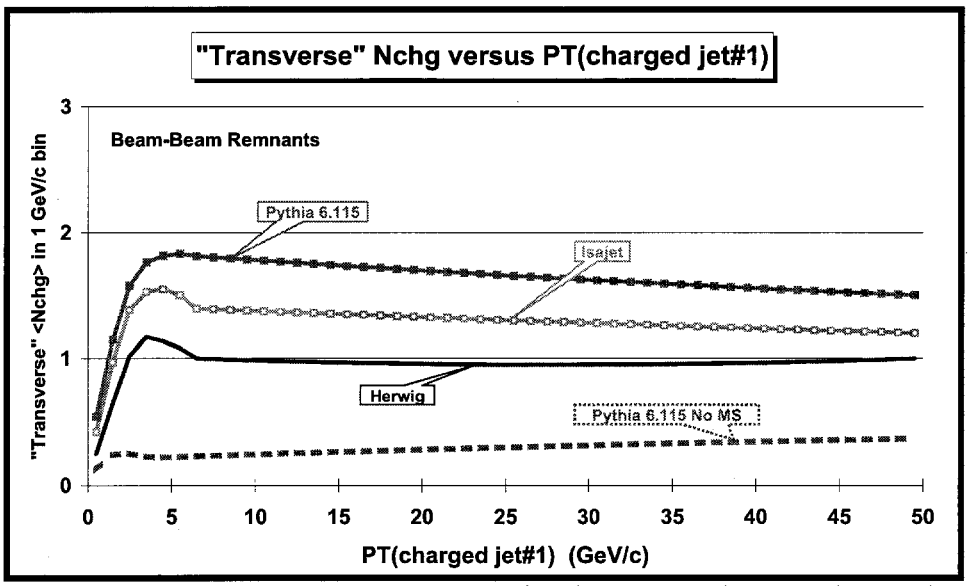

FIG. 36. QCD hard scattering Monte-Carlo predictions from HERWIG, ISAJET, PYTHIA 6.115, and PYTHIA 6.115 with no multiple parton scattering (No MS) for the average number of charged particles ($p_T > 0.5\,\mathrm{GeV/c}$, $|\eta| < 1$) as a function of P_{T1} (leading charged jet) for the transverse region defined in Fig. 14 arising from the break-up of the beam particles (beam-beam remnants). For PYTHIA the beam-beam remnants include contributions from multiple parton scattering (see Fig. 2).

There are two reasons why the hard scattering component of ISAJET is different from HERWIG and PYTHIA. The first is due to different fragmentation schemes. ISAJET uses independent fragmentation, which produces too

many soft hadrons when partons begin to overlap. The second difference arises from the way the QCD Monte-Carlo models produce parton showers. ISAJET uses a leading-log picture in which the partons within the shower are ordered according to their invariant mass. Kinematics requires that the invariant mass of daughter partons be less than the invariant mass of the parent. HERWIG and PYTHIA modify the leading-log picture to include color coherence effects which leads to angle ordering within the parton shower. Angle ordering produces less high p_T radiation within a parton shower which is what is seen in Fig. 35. Without further study, we do not know how much of the difference seen in Fig. 35 is due to the different fragmentation schemes and how much is due to color coherence effects.

The beam-beam remnant contribution to the transverse $\langle N_{\rm chg}\rangle$ is different for each of the QCD Monte-Carlo models. This can be seen in Fig. 36 where we compare directly the beam-beam remnant component of the transverse $\langle N_{\rm chg}\rangle$ from ISAJET, HERWIG, PYTHIA 6.115, and PYTHIA with no multiple parton interactions. Since we are considering only charged particles with $p_T > 0.5\,{\rm GeV/c}$, the height of the plateaus in Fig. 36 is related to the transverse momentum distribution of the beam-beam remnant contributions. A steeper p_T distribution means less particles with $p_T > 0.5\,{\rm GeV/c}$. PYTHIA uses multiple parton scattering to enhance the underlying event and we have included these contributions in the beam-beam remnants. For PYTHIA the height of the plateau in Fig. 36 can be adjusted by adjusting the amount of multiple parton scattering. HERWIG and ISAJET do not include multiple parton scattering. For HERWIG and ISAJET the height of the plateau can be adjusted by changing the p_T distribution of the beam-beam remnants.

We will now study the p_T distribution of the beam-beam remnants by examining the transverse momentum distribution of the charged particles produced in the transverse region.

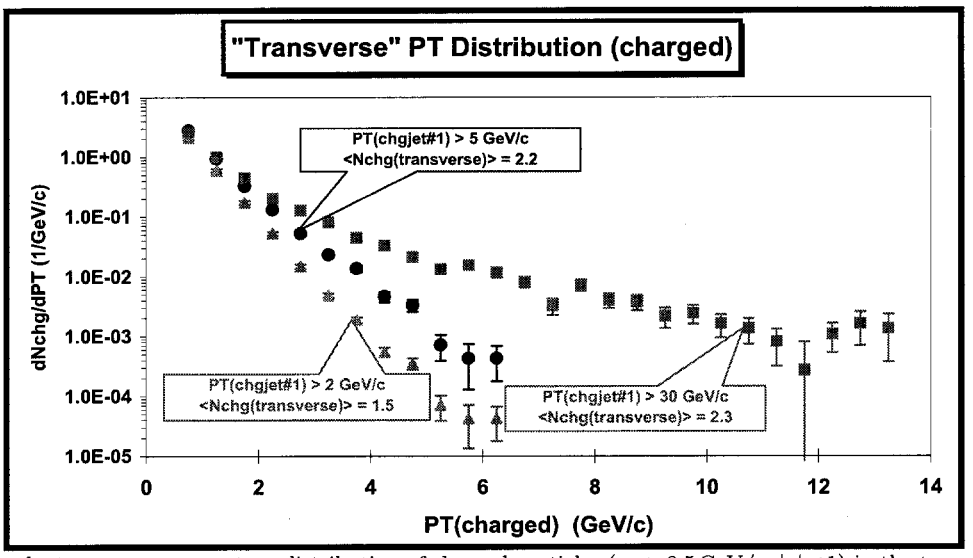

FIG. 37. Data on the transverse momentum distribution of charged particles ($p_T > 0.5\,{\rm GeV/c}$, $|\eta| < 1$) in the transverse region defined in Fig. 14 for $P_{T1} > 2\,{\rm GeV/c}$, $5\,{\rm GeV/c}$, and $30\,{\rm GeV/c}$, where chgjet#1 is the leading charged particle jet. The $P_{T1} > 2\,{\rm GeV/c}$ and $5\,{\rm GeV/c}$ points are Min-Bias data and the $P_{T1} > 30\,{\rm GeV/c}$ are JET20 data. Each point corresponds to the charged particle density $d\langle N_{\rm chg}\rangle/dp_T$ and the integral of the distribution gives the average number of charged particles in the transverse region, $\langle N_{\rm chg}({\rm transverse})\rangle$. The errors on the (uncorrected) data include both statistical and correlated systematic uncertainties. (Note the logarithmic scale on the vertical axis.)

B. Transverse p_T Distribution

Fig. 37 shows the data on the transverse momentum distribution of charged particles ($p_T > 0.5\,{\rm GeV/c}$ and $|\eta| < 1$) in the transverse region defined in Fig. 14. The $P_{T1} > 2\,{\rm GeV/c}$ and $5\,{\rm GeV/c}$ points are Min-Bias data and the $P_{T1} > 30\,{\rm GeV/c}$ points are JET20 data. Each point corresponds to the charged particle density $d\langle N_{\rm chg}\rangle/dp_T$ and the integral of the distribution gives the average number of charged particles in the transverse region, $\langle N_{\rm chg}({\rm transverse})\rangle$. Since these distributions fall off sharply as p_T increases, it is essentially only the first point at low p_T that determines $\langle N_{\rm chg}({\rm transverse})\rangle$. The approximately constant plateau seen in Fig. 28 is a result of the low p_T points in Fig. 37 not changing much as P_{T1} changes. However, the high p_T points in Fig. 37 do increase considerably as P_{T1} increases. This effect cannot be seen by simply examining the average number of transverse particles. Fig. 37 shows the growth of the hard scattering component in the transverse region (i.e., three or more hard scattering jets).

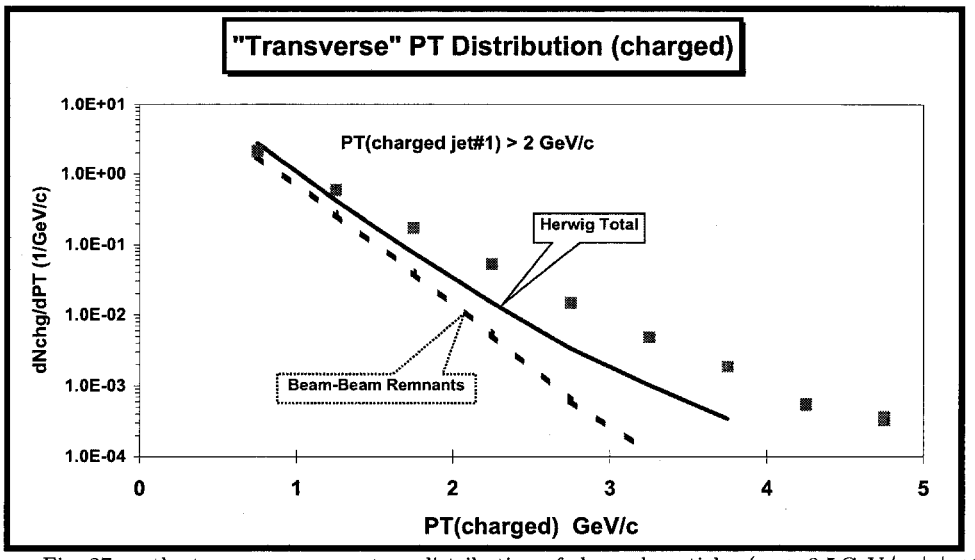

FIG. 38. Data from Fig. 37 on the transverse momentum distribution of charged particles ($p_T > 0.5\,\mathrm{GeV/c}$, $|\eta| < 1$) in the transverse region defined in Fig. 14 for $P_{T1} > 2\,\mathrm{GeV/c}$ compared to the QCD hard scattering Monte-Carlo predictions from HERWIG. The dashed curve shows the contribution arising from the break-up of the beam particles (beam-beam remnants) predicted by HERWIG. (Note the logarithmic scale on the vertical axis.)

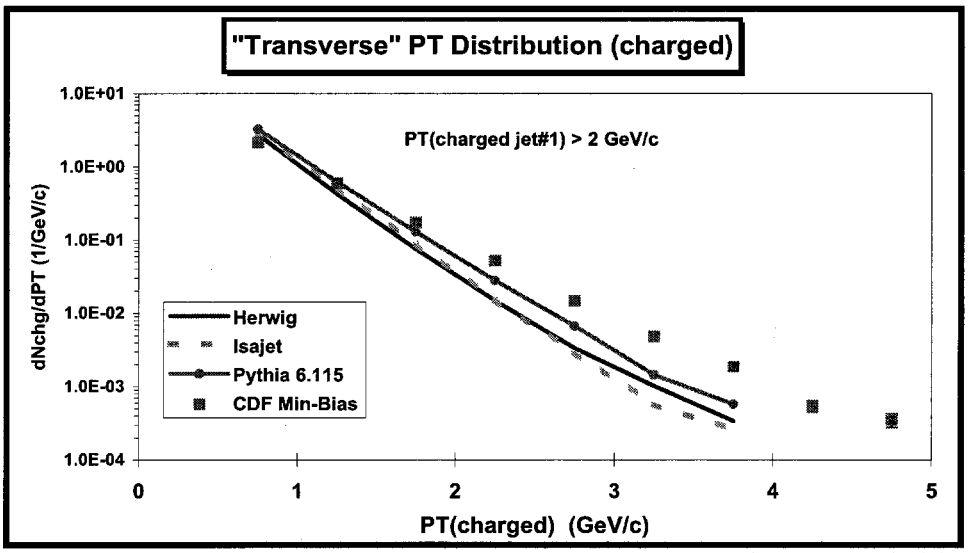

FIG. 39. Data from Fig. 37 on the transverse momentum distribution of charged particles ($p_T > 0.5\,\mathrm{GeV/c}$, $|\eta| < 1$) in the transverse region defined in Fig. 14 for $P_{T1} > 2\,\mathrm{GeV/c}$ compared to the QCD hard scattering Monte-Carlo predictions from predictions from HERWIG, ISAJET, and PYTHIA 6.115. (Note the logarithmic scale on the vertical axis.)

For low values of P_{T1} the p_T distribution in the transverse region is dominated by the beam- beam remnant contribution with very little hard scattering. This can be seen in Fig. 38 which shows both the beam-beam remnant component and the total prediction of HERWIG for $P_{T1} > 2\,\mathrm{GeV/c}$. At low values of P_{T1} the p_T distribution in the transverse region measures directly the p_T distribution of the beam-beam remnants. Fig. 39 compares the predictions of HERWIG, ISAJET, and PYTHIA with the data from Fig. 37 for $P_{T1} > 2\,\mathrm{GeV/c}$. Both ISAJET and HERWIG have the wrong p_T dependence due to beam-beam remnant components that fall off too rapidly as p_T increases. PYTHIA does a better job, but is still too steep. It is, of course, understandable that the Monte-Carlo models might be slightly off on the parameterization of the beam-beam remnants. This component cannot be calculated from perturbation theory and must be determined from data.

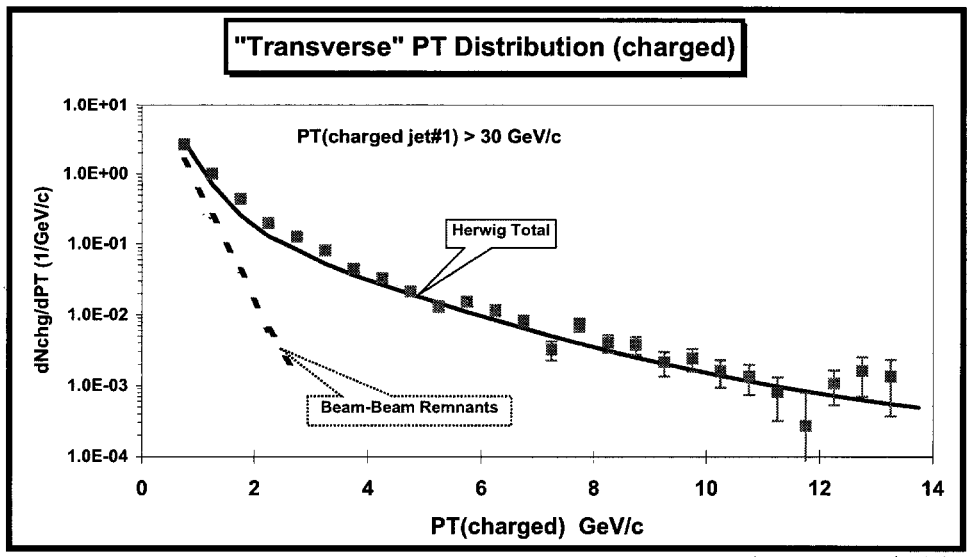

FIG. 40. Data from Fig. 37 on the transverse momentum distribution of charged particles ($p_T > 0.5\,\mathrm{GeV/c}$, $|\eta| < 1$) in the transverse region defined in Fig. 14 for $P_{T1} > 30\,\mathrm{GeV/c}$ compared to the QCD hard scattering Monte-Carlo predictions from HERWIG. The dashed curve shows the contribution arising from the break-up of the beam particles (beam-beam remnants) predicted by HERWIG. (Note the logarithmic scale on the vertical axis.)

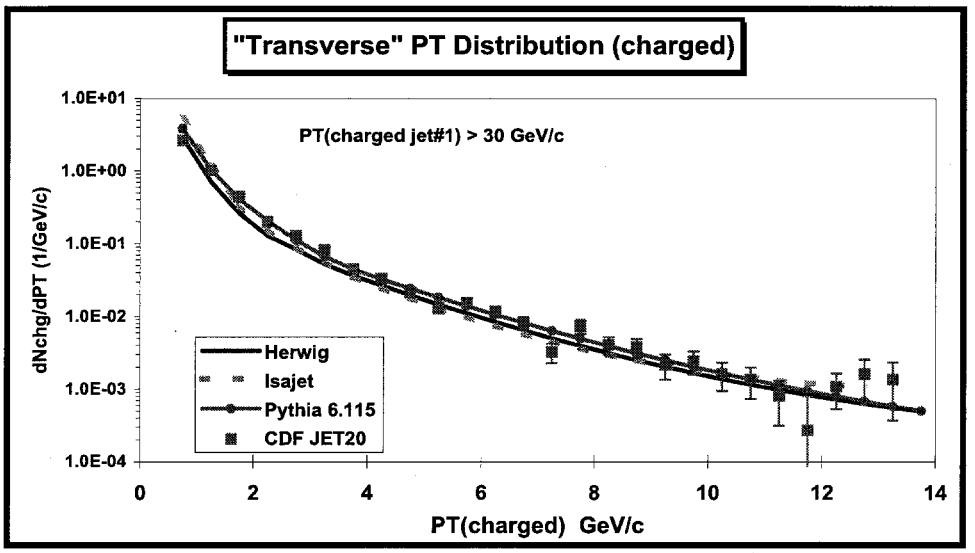

FIG. 41. Data from Fig. 37 on the transverse momentum distribution of charged particles ($p_T > 0.5\,\mathrm{GeV/c}$, $|\eta| < 1$) in the transverse region defined in Fig. 14 for $P_{T1} > 30\,\mathrm{GeV/c}$ compared to the QCD hard scattering Monte-Carlo predictions from predictions from HERWIG, ISAJET, and PYTHIA 6.115. (Note the logarithmic scale on the vertical axis.)

Fig. 40 shows both the beam-beam remnant component and the total prediction of HERWIG for $P_{T1} > 30\,\mathrm{GeV/c}$. Here there is a large hard scattering component corresponding to the production of more than two large p_T jets. In Fig. 41 we compare the predictions of HERWIG, ISAJET, and PYTHIA 6.115 with the data from Fig. 37 for $P_{T1} > 30\,\mathrm{GeV/c}$. All the models do well at describing the high p_T tail of this distribution. However, ISAJET produces too many charged particles at low p_T. This is a result of the wrong p_T dependence for the beam-beam remnant contribution and from an overabundance of soft particles produced in the hard scattering. This shows that the large rise in the transverse charged multiplicity from the hard scattering component of ISAJET seen in Fig. 35 comes from soft particles. This is to be expected from a model that employs independent fragmentation such as ISAJET. Independent fragmentation does not differ much from color string or cluster fragmentation for the hard particles, but independent fragmentation produces too many soft particles.

VI. SUMMARY AND CONCLUSIONS

We have studied both leading charged jet observables and global observables where to fit the data the QCD Monte-Carlo models have to correctly describe the overall event structure. Our summary and conclusions are as follows.

The Evolution of Charged Particle Jets

We see evidence of charged particle clusters (i.e., charged particle jets) in the Min-Bias data. These charged particle jets become apparent somewhere around P_{T1} of about 2 GeV/c with, on the average, about 2 charged particles with $p_T > 0.5$ GeV/c and $|\eta| < 1$ and grow to, on the average, about 10 charged particles with $p_T > 0.5$ GeV/c and $|\eta| < 1$ at $P_{T1} = 50$ GeV/c. The QCD hard scattering models describe quite well (although not perfectly) leading jet observables such as the multiplicity distribution of charged particles within the leading charged jet, the size of the leading charged jet, the radial distribution of charged particles and transverse momentum around the leading charged jet direction, and the momentum distribution of charged particles within the leading charged jet. In fact, the QCD hard scattering Monte-Carlo models agree as well with 5 GeV/c charged particle jets as they do with 50 GeV/c charged particle jets. The charged particle jets in the Min-Bias data are simply a continuation (down to small p_T) of the high transverse momentum charged jets observed in the JET20 data.

The Underlying Event

A hard scattering collider event consists of large transverse momentum outgoing hadrons that originate from the large transverse momentum partons (outgoing jets) and also hadrons that originate from the break-up of the proton and antiproton (beam-beam remnants). The underlying event is formed from the beam-beam remnants, initial-state radiation, and possibly from soft or semi-hard multiple parton interactions. Our data show that the average number of charged particles and average charged scalar p_T sum in the underlying event grows very rapidly with the transverse momentum of the leading charged particle jet and then forms an approximately constant plateau for $P_{T1} > 5$ GeV/c. The height of this plateau is at least twice that observed in ordinary soft collisions at the same corresponding energy.

None of the QCD Monte-Carlo models we examined correctly describe all the properties of the underlying event seen in the data. HERWIG and PYTHIA 6.125 do not have enough activity in the underlying event. PYTHIA 6.115 has about the right amount of activity in the underlying event, but as a result produces too much overall charged multiplicity. ISAJET has a lot of activity in the underlying event, but with the wrong dependence on P_{T1}. Because ISAJET uses independent fragmentation and HERWIG and PYTHIA do not, there are clear differences in the hard scattering component (mostly initial-state radiation) of the underlying event between ISAJET and the other two Monte-Carlo models. Here the data strongly favor HERWIG and PYTHIA over ISAJET.

At low values of P_{T1} the p_T distribution in the transverse region measures directly the p_T distribution of the beam-beam remnants. The beam-beam remnant component of both ISAJET and HERWIG has the wrong p_T dependence. ISAJET and HERWIG both predict a p_T distribution for the beam-beam remnants that is too steep. With multiple parton interactions included, PYTHIA does a better job but still has a p_T distribution for the beam-beam remnants that is slightly too steep. It is, of course, understandable that the Monte-Carlo models might be somewhat off on the parameterization of the beam-beam remnants. This component cannot be calculated from perturbation theory and must be determined from data. With what we have learned from the data presented here, the beam-beam remnant component of the QCD hard scattering Monte-Carlo models can be tuned to better describe the underlying event in proton-antiproton collisions.

Acknowledgements

We thank the Fermilab staff and the technical staffs of the participating institutions for their vital contributions. This work was supported by the U.S. Department of Energy and National Science Foundation; the Italian Istituto Nazionale di Fisica Nucleare; the Ministry of Education, Science, Sports and Culture of Japan; the Natural Sciences and Engineering Research Council of Canada; the National Science Council of the Republic of China; the Swiss National Science Foundation; the A. P. Sloan Foundation; the Bundesministerium fuer Bildung und Forschung, Germany; the Korea Science and Engineering Foundation (KoSEF); the Korea Research Foundation; and the Comision Interministerial de Ciencia y Tecnologia, Spain.

---

[1] G. Marchesini and B. R. Webber, Nucl. Phys **B310**, 461 (1988); I. G. Knowles, Nucl. Phys. **B310**, 571 (1988); S. Catani, G. Marchesini, and B. R. Webber, Nucl. Phys. **B349**, 635 (1991).

[2] F. Paige and S. Protopopescu, BNL Report, BNL38034, 1986 (*unpublished*), version 7.32.
[3] T. Sjostrand, Phys. Lett. **157B**, 321 (1985); M. Bengtsson, T. Sjostrand, and M. van Zijl, Z. Phys. **C32**, 67 (1986); T. Sjostrand and M. van Zijl, Phys. Rev. **D36**, 2019 (1987).
[4] F. Abe *et al.* ., Nucl. Instrum. Methods, **A271**, 387 (1988); F. Bedeshi *et al.* ., Nucl. Instrum. Methods, **A268**, 50 (1988).
[5] F. Abe *et al.* , Phys. Rev., **D56**, 3811 (1997); F. Abe *et al.* ., Phys. Rev. Lett.,**79**, 584 (1997).
[6] F. Abe *et al.* , Phys. Rev., **D41**, 2230 (1990).